Author's response

We thank the reviewers for their comprehensive review of our submitted manuscript, giving a number of comments and suggestions for improvements. In the following, we respond to each of the comments and amendments, and, where applicable, added our changes to the revised manuscript (attached). We feel that the presented changes will greatly improve our submission in order to provide it in a format acceptable for publication within this Journal.
We also would like to note that, as part of the review process, we introduced a new figure, which is why the figure numbers have changed in the revised manuscript. Moreover, the line numbers have changed essentially. Therefore, in the following author response, all changes refer to the line numbers (in square brackets) of the revised and marked-up manuscript attached to the end of this document.

Author response to reviewer 1

Referee: Anett Blischke (ÍSOR Iceland Geosurvey)

General remarks and main points:

- *Interesting study that add to the borehole / core in-situ lab experiments for metamorphic rock settings, which is important for extending the global calibration database for deeply buried metamorphic rocks and their understanding.*
- *This aim was however (as first stated in the introduction) to improve the imaging of thrust zones and the understanding of the deeper orogenic processes and tectonic evolution? How does the manuscript relate to that project objective? I think this needs a small revision of the introduction to fit the study that in itself has a good closure.*
- *I bring in quite a few suggestions, but hope they help to make this a good paper and contribution.*
- *Looking forward to see the revised manuscript.*

Abstract:
Has all the info, still possibly sort the sentences.
- *Where?*
- *What objective?*
- *Doing What?*
- *How?*
- *Resulting?*
- *What didn´t work?*
- *What did?*
- *Why are the study results important?*

Please re-arrange specifically this passage, I am getting confused what are the results that didn't work and what did. Always better to end on the results that did work:
"The core and downhole velocities deviate by up to 2 km/s. However, velocities of mafic rocks are generally in close agreement. Seismic anisotropy increases from about 5 to 26 % at depth, indicating a transition from gneissic to schistose foliation. We suggest that differences in the core and downhole velocities are most likely the result of microcracks mainly due to depressurization. Thus, seismic velocity can help to identify mafic rocks on different scales whereas the velocity signature of other lithologies is obscured in core-derived velocities. Metamorphic foliation on the other hand has a clear expression in seismic anisotropy."

> We have modified the abstract accordingly, in order to better point out the motivation and main results of the publication:

"[…] For some intervals of the COSC-1 borehole, the core and downhole velocities deviate by up to 2 km/s. These differences in the core and downhole velocities are most likely the result of microcracks mainly due to depressurization. However, the core and downhole velocities of the intervals with mafic rocks are generally in close agreement. Seismic anisotropy measured on laboratory samples increases from about 5 to 26 % at depth, correlating with a transition from gneissic to schistose foliation. Metamorphic foliation on the other hand has a clear expression in seismic anisotropy. These results will aid in the evaluation of core-derived seismic properties of high-grade metamorphic rocks at the COSC-1 borehole and elsewhere."

Please just refer to the COSC-1 borehole consistently.

We have revised and adjusted all references to the borehole to "COSC-1". Where we explicitly refer to the general project COSC, this is clarified in the text.

Introduction:

General, please check that references are placed, were facts and introductions are stated.

Done.

Your primary objective is to "… to improve our understanding of the deeper orogenic processes and tectonic evolution." (first paragraph)
Then follows the geophysical experiments that led to this study (REF?), specifically seismic reflection data and imaging of that thrust zone (REF?), and how does better sub-surface imaging than improve the understanding of the tectonic evolution based on core data?

See comment below.

Suggest to rephrase the primary objective that than follows well into the paragraphs (L33-39), as here it is a lithological / stratigraphic objective and not the thrust zone is described. Knowing the stratigraphy and the rocks petrophysical properties would lead to better seismic reflection data processing and imaging for example.

We agree that the objective of this particular study is not clearly separated from the primary ("long-term") objective of the COSC drilling project. As pointed out by the reviewer, the ultimate aim addressed by the COSC project is the understanding of the deeper orogenic processes and tectonic evolution of the Scandinavian Caledonides. Seismic reflection data provides one tool to image subsurface and to interpret these structures (including thrust zones and nappe stacks) at depth. Especially, by knowing the physical properties of the associated rocks at depth this can help to better constrain reflections and aid the processing and interpretation of these reflection profiles.

We have revised and rearranged the introduction in order to point out which is the long-term project aim and how our study contributes to it (objective of this study versus COSC drilling project aims). Essentially, this has required some sentences to be rephrased or moved.

If there are only 2 primary projects of this kind KTB or the CCSD, why not say so and spell them out? What about the study by Zappone et al. (2000) for the Iberian, or the Kola Borehole Kern et al. (2001)? (Kern, H. & Popp, Till & Gorbatsevich, Feliks & Zharikov, Andrey & Lobanov, K. & Smirnov, Yu. (2001). Pressure and temperature dependence of V P and V S in rocks from the superdeep well and from surface analogues at Kola and the nature of velocity anisotropy. Tectonophysics. 338. 113-134. 10.1016/S0040-1951(01)00128-7.)

Certainly, there are more than two studies of such kind. Our purpose was to highlight especially these two, which are of comparable geological/tectonic setting with a similar high core recovery. We agree, however, we have added additional references in order to provide a more concise overview of the related literature and background. [l. 55 ff.]

We therefore have explicitly named these projects and, furthermore, added the following references:

- Golovataya, O. S., Gorbatsevich, F. F., Kern, H. and Popp, T.: Properties of some rocks from the section of the Kola ultradeep borehole as a function of the P-T parameters, Izv. Phys. Solid Earth, 42(11), 865–876, doi:10.1134/S1069351306110012, 2006.
- Sun, S., Ji, S., Wang, Q., Xu, Z., Salisbury, M. and Long, C.: Seismic velocities and anisotropy of core samples from the Chinese Continental Scientific Drilling borehole in the Sulu UHP terrane, eastern China, J. Geophys. Res. Solid Earth, 117(B1), n/a-n/a, doi:10.1029/2011JB008672, 2012.
- Kern, H., Schmidt, R., Drilling, T. P.-S. and 1991, U.: The velocity and density structure of the 4000 m crustal segment at the KTB drilling site and their relationship to lithological and microstructural, Sci. Drill., 2, 130–145, 1991.
- Elbra, T., Karlqvist, R., Lassila, I., Haeggström, E. and Pesonen, L. J.: Laboratory measurements of the seismic velocities and other petrophysical properties of the Outokumpu deep drill core samples, eastern Finland, Geophys. J. Int., 184(1), 405–415, 2011.

L48-51: *This sentence I would suggest moving up front to follow with the supporting role of this project to better understanding of thrust zone and metamorphic settings.*

Moved sentences/paragraph up front as suggested. [l 40. ff.]

L53-58: *Isn't this better placed in the methods section?*

In order to give the reader short agenda and an idea of the following sections, we have briefly introduced the applied methods. We think this is a worthwhile extension of the introduction.

Section 1.1: *This is a good concise overview but using the geological map and cross-section with the COSC-1 borehole projected on it, would really help to get the borehole's geological settings placed in the reader's head, especially if one isn't that familiar with the area. This gives an option to show that main subdivisions described by Lorenz et al. (2015a) that leads well into the smaller scale core-based experiment.*

We agree and have added an additional subfigure to get the reader more familiar with the regional setting. See also comment on Figure 1 in the figures subsection further below.

L75: *What type of deformations (fracturing / folding / cataclastic)?*

Rocks of the COSC-1 borehole predominantly exhibit ductile shear deformation with signs of mylonitic deformation and micro-folding.

Amended sentence to [l. 95]: "[…] (2) an extensive (ductile shear) deformation zone prevails between […]".

<u>Data and methods:</u>

Please be more specific in describing what downhole logging data in the intro, you have them in Table 1. It would be good to briefly just state that these included short-spaced sonic and zero-offset VSP in the text with the appropriate referencing and reference to Figure 2, this way it's clear from the start of reading this chapter.

We have stated and specified the used data [l. 104 ff.]: "[...] from a multi-sensor core log (MSCL) and downhole data including short-spacing sonic log and zero-offset VSP […]".

L98: *see Table 2 and Appendix A1. I am a bit missing a Figure that shows the known geology with the core section and sample location. This is a preference for people that prefer to see the graphic setup of the borehole samples. Just a suggestion, but this way it would be easier to follow who measured what at sample depth, with higher and lower reflectivity zone based on VSP, etc.? This could even be part of Appendix A1 if the number of figures has to stay. Please see Figures 2 by Zappone et al. (2000).*

We understand the reviewers suggested to show the geology of the samples in a figure. We therefore have extended Figure 1 showing the tectonic-stratigraphic successions in the survey area. Moreover, the lithological units and the exact depth of the samples are shown in Figure 11, which is why we prefer not to add another figure for the sample positions.

L104-107: *Could you indicate this in Figure 4, there would be enough space for the Core MSCL image, indicating the xyz structural axis to the foliation plane. Please see Figure 4 by Zappone et al. (2000).*

We agree that it is useful for the reader to understand the relation between the structural axes and the core plug measurements. Indicating this in Figure 2, however, next to the Core MSCL picture might give a wrong impression that the core/borehole is always perpendicular to the foliation plane, which is not always the case. Especially, with Figure 2 we intend to provide the more general case highlighting only the different scale and measurement conditions. Thus, we prefer to rather implement the structural coordinate system in another figure together with a raw data example (see comment on Figure 5 and L224).

Good explanation of the Figure 3 and the method.

L131-133: *What temperature was at the 2500m? T_{2500m} = (20 °C/km * 2,5 km) + 6,4 °C = 56.4°C? I am just wondering as Table 2 indicates a depth range 400-2460m, which in turn would indicate a general linear in-situ temperature range between 14,4-55,6 °C. So why is room temperature acceptable, or has it been shown that temperature does not affect the measurements. If so, please state and reference that.*

For this study, of highly consolidated metamorphic rocks, thermal effects on velocity and anisotropy can be neglected (e.g., Kern 1990). Especially, for the investigated depth and temperature range these effects are small compared to pressure effects (compare with Zappone et al. (2000)). The following paragraph clarifies this.

We have added the following paragraph, for clarification [l 155 ff.]:
"Generally, seismic velocities decrease with temperature (e.g., Schön (1996), Motra and Stutz (2018)). However, at very low temperatures (< 100 °C), like we observe in the COSC-1 borehole, this effect can be neglected (Kern (1978)). Moreover, the measured pressure to temperature increment (about 1.5 MPa/K) in the COSC-1 borehole is sufficiently high to prevent thermal microcracking (Kern (1990))."

Based on lab work by Mobarek (1971), would the Vp values be slightly low based on temperature increase. Of course, those tests were done on dry sandstone, and it would be good at least to describe how temperature would affect the lab results.

We agree that the seismic velocity measurements can show thermal effects depending on the investigated rock types. In particular, this effect is more pronounced in highly porous rocks as described in the work by Mobarek (1971). However, as we described above, for low-porous, consolidated rocks at lower crustal depths and low geothermal gradient the effect is outweighed by the effect of pressure as demonstrated by the extensive work of Kern. For completeness, we have added a short description of the general effect as stated in the previous comment.

Possibly use ranges from similar studies in comparison (e.g. Iberian Peninsula)?

Please see comment to L131-133 above.

Motra, Hem & Stutz, Hans. (2018). Geomechanical Rock Properties Using Pressure and Temperature Dependence of Elastic P- and S-Wave Velocities. Geotechnical and Geological Engineering. 10.1007/s10706-018-0569-9.

We addressed the thermal effect in the above mentioned paragraph, and we have added the reference to the manuscript [l. 155 ff.].

L144-154: *So what are you saying, are you applying this method or not? It's just the explanation and reasoning – the data trend measured vs. empirical looks convincing – perhaps just rephrase slightly to be clear.*

We have rephrased this paragraph for clarification as follows:

Amended L144 [l. 170]: "We used the relationship derived by Ji et al. (2007) to calculate velocity-pressure curves for each of our 10 core plugs (Fig. 5)."

Amended L149 [l. 175]: "Wenning et al. (2016) used a slightly different relation for their six samples, proposed by Wepfer and Christensen (1991)."

Removed L151-153: "However, based on [...]"

Rephrased L150-154 [l. 176 ff.]: "For most applications aiming to determine the linear high-pressure part and intrinsic anisotropy both relations give consistent results. However, the inherent zero-boundary condition of Wepfer and Christensen's relation may lead to errors in the extrapolation of the non-linear low-pressure part, why we used the relationship by Ji et al. (2007) instead."

L156: *Different in what?*

We have added the following sentence, for clarification [l. 184 ff.]:
"These representations are generally based on a fractional difference of the maximum and minimum measured velocities but distinguish in the applied denominator."

Section 2.2: *As you do not reference the setup anywhere in this section, either add a figure explaining this as in Figure 3 for the lab setup or point to the appropriate reference that one can go to for understanding the setup. Is this your method, then state this, or refer to the method shown as a reference? You have done that for your lab setup and the VSP.*

As this is not our method, we have added the following references that describe the applied method [l. 200]:

- "Breitzke, M. and Spieß, V.: An automated full waveform logging system for high-resolution P-wave profiles in marine sediments, Mar. Geophys. Res., 15(4), 297–321, doi:10.1007/BF01982387, 1993."
- "Weber, M. E., Niessen, F., Kuhn, G. and Wiedicke, M.: Calibration and application of marine sedimentary physical properties using a multi-sensor core logger, Mar. Geol., 136(3–4), 151–172, doi:10.1016/S0025-3227(96)00071-0, 1997."

L179: *… accordingly to what?*

This refers to the detected signal-to-noise ratio during the measurement. We have rephrased the sentence to [l. 209]: "[...] automatically, to ensure a good signal-to-noise ratio for the automatic picker."

L214: *… at 0,5 m spacing?*

To clarify the meaning of the different receiver spacing, we have rephrased the sentence [l. 244 ff.]: "[...] which is defined by the applied receiver spacing (2 m). The distance over which the velocity is averaged is, thus, four times larger than for the downhole sonic log (with 0.5 m receiver spacing)."

L219: *I would leave this and state "used in our study". If you start mentioning "best case" than this naturally follows the question, what the low and high cases are that need explaining.*

We have clarified and corrected this by replacing "(best case)" with "(Rayleigh resolution limit)" [l. 251].

<u>Results:</u>

L224: *Here it would have been nice to see the data plotted of Table 2, as described as the applied method on Figure 5. These are the main results that all following conclusion is based on.*

In Figure 5, we prefer to present a more generic depiction that outlines the applied method and derived data from the general measurements.

We agree that by showing the raw data of Vp and AVp measured as a function of confining pressure would benefit the understanding of the applied processing and method (Figure 5). We therefore have introduced one additional figure (i.e., Figure 6) showing a raw data example, which would integrate well with the applied method/processing part. In this data example (Figure 6), we have also added the structural coordinate system determined for each sample as suggested in the comment on L104-107. See also comment on Figure 5 in the figures section. We also prefer not adding any additional graphs because they won't add to the publication's objectives. They will, however, be part of another publication which focuses on the seismic anisotropy behavior.

At the moment the Table 2 has only the final results Vp0, VpAP, VpLP vs. build up pressure for each vector and mean, based on your measurements and calculations. Did you double check by including measurements for increased pressure that gives a step by step series measured Vp that would demonstrate with your data what was explained in Figure 5 and the methods?
Please see example here: https://academic.oup.com/gji/article-pdf/187/3/1393/1694975/187-3-1393.pdf

We have incorporated a data example that shows the two pressure cycles in the above mentioned new figure.

L232: *Do you mean "core plug axial measurements"?*

That is correct. We rephrased the sentence accordingly [l. 263]:
"[...] from the arithmetic mean of the three axial core plug measurements (x, y, and z plug). It represents [...]"

L250-261: *Here it would be good to point out that core-derived Vp relates to the whole core log measurements at surface conditions, whereas the Sonic-VSP Log are measured has the hydrostatic pressure in the borehole and the in situ rock.*

As this part of the paper describes the results we prefer not to interpret and explain the data. However, in order to explain the reader the impact of the different measurement approaches, we included the following sentence [l. 282 ff.]:
"As core-derived Vp relates to the whole core log measurements at surface conditions, whereas the sonic and VSP log are measured has the hydrostatic pressure in the borehole and the in situ rock (cf. Fig. 2),

we expected the downhole measurements to show potentially higher values. Our data shows that there is neither a […] “

I would suggest to point out the depth intervals, where the logged rock velocity is opposite in the general trend of the VSP-Log data that follows the lithology changes - add density log alongside? What about fault / fracture zones that would stand out of the rock matrix investigated?

We have specified the depth intervals where the MSCL core velocity is opposite. Thus, we added some examples in brackets to the observation previously made in the results section [l. 296 ff.].

***L262-263:** Please be specific that the reader can follow, e.g. VpAP with the core logged velocity at surface, the VpLP to the VSP-Log data.*

To avoid any confusion, we have added the abbreviations in brackets, where it is referred to. [l. 299 ff.]

I would suggest pointing out the samples that are outliers / slightly off, e.g. 106.1; 143.1; 243.2; 361.2; 641.5; 661.3; or 691.1
This is more specific than to negate an entire interval, as the shallow data do not miss-match that much in comparison to the deeper interval.
You are doing this for the VpAP in the next section below.

We have included the reviewer’s suggestion accordingly and specified/named those samples that deviate. [l. 308 ff.]

***L269:** Why might this be? Are those sample much fractured?*

There are different possible reasons. Most likely this points to a stronger effect of microcracks that reduces the core velocity stronger than for the other lithologies. This hypothesis is again pointed out in the discussion. Here, however, we propose to only focus on the observations of the data and results.

***L290:** What do you mean with improper relationship? The matches are close/reasonable for examples B, E, F, and D, but samples A and C are consistently lower. In comparison to the lithology, is that seen along the borehole at other depths as well?*

We agree that this was not properly stated. We have removed the reasoning [l. 331] from the results and only point to the observation of the “lower sample velocities (VpAp)”. Possible scenarios that again explain the data are part of the discussion.

***L295:** Why keep working with that example if you do not show it? Is it possible to add the example to the display in Figure 11?*

The “not shown” examples have very similar results and are representative for the shown examples. We therefore have removed “not shown” and instead refer to Figure 11 (formerly 10). In order to keep the proportion and clarity of the figure, we rather prefer to show examples of the unique samples in Figure 11.

***L303:** Why might this be? Please explain.*

The low core velocity is similar to what was observed for the felsic gneiss sections, and thus is a result of the schistose texture, which may favor the development of oriented microcracks. We have explained and discussed this result in the discussion [l. 429].

L329-330: *Is that also in reference to your final figure 12? You are using 106-1 to 193-2 format for the other intervals with selected samples.*

In this paragraph, we only refer to the sample data of the laboratory measurements. Later on, these are also represented in Figure 13 [formerly Fig. 12], where we also took the other logs into account. This is again pointed out in later in the discussion, noting that the highlighted regions are based on the regions indicated by the anisotropy-depth profile [l. 482]:
"[…] lithology, and which are consistent with the zones indicated by the anisotropy-depth profile as discussed earlier."

Moreover, we have adjusted the description of the lithological units and added the sample names as suggested by the reviewer [l. 373 ff]:
"Assuming that the point measurements sufficiently represent the core, we distinguished four different zones based on the anisotropy depth profile (Fig. 8). They correspond to the following major lithological units: […]"

L346: *Just Figure 10?*
Isn´t this best displayed on Figure 12?

This is correct and both visible on Fig.11 and Fig. 12. Thus, we also have added Figure 12 (formerly Fig. 11) to the reference list in here. We see the same again in Figure 13 (formerly Fig. 12, which, however, will be introduced again later in the discussion, why we prefer to exclude at this point. [l. 393]

L365: *What about saturated micro-fractures that are measured as well within the matrix rock?*

Saturated micro-fractures such as related with secondary porosity should give a similar explanation. In case of a preferred orientation of the micro-fractures this can again affect the anisotropy behavior of the rock. Here, we do neglect the case of open micro-fractures under in situ conditions, because we consider the lithostatic pressure to be high enough to close microfractures/-cracks in the core samples.

L374: *... for X points out of X of VpLP.*

We have specified this observation and added how many and which of the measurements show this behavior [l. 421].

L392: *Are you talking about the Core Log" or Vp0, VpAP, and VpLP as a group of VpLP specifically? Might be good to specify at the beginning of the paragraph, so the reader doesn´t mix up the two data sets.*

Here, we particularly refer to the core and downhole logs from MSCL and sonic, respectively. As the reviewer suggested, we have specified this as follows [l. 440]:
"Core and downhole velocity measurements using MSCL and sonic tools, respectively, are subject to different scales […]"

L418: *Possibly marked these 10% as depth intervals on Figure 10 and 12.*

These 10% only refers to an approximation of the cumulative number of fractures in the cores due to core transitions (artificially broken core pieces to fit the core boxes) and natural fractures detected from televiewer analysis from Wenning et al. (2017). We have specified that these refer to the raw core data measured by the MSCL [l. 464].

L460: *Definitely revise your introduction to focus the study on the matrix primarily and influences of fractures / micro-fractures,* As pointed out by the reviewer we have revised the introduction and included a part highlighting the importance of microcracks [l. 44] and indicated that these may have a considerable effect on the investigated seismic properties [l. 46].

Figures and table:

Figures and Tables are clearly structured, and features displayed well visible, still here are a few comments and suggestions.

- ***Figure 1:***
  - *The figure looks too much as a copy – past. You could ask to get a GIS version / emf draft of that map and leave out all the lines and info that doesn't matter, such as roads, power lines. Just focus on the geological- and tectonic, and borehole location. Standard is – if you have something displayed on your map, you should include that in the legend.*

    As suggested we have cleaned-up the map (remove any unimportant information), and added the missing legend entries. Furthermore, we have added subfigures of the regional tectonostratigraphy and seismic profile to better depict the geological setting and location of the COSC-1 borehole. The colors are organized in a way that one can easily depict the different tectonic units throughout the subfigures (e.g., orange colors refer to Seve Nappe Complex, etc). See figure below.

  - *Is there any profile section available to show how the borehole is placed and intersects the thrust zone? There are quite a few references listed that show that this should be available (Gee et al., 1985a,b; 2008, 2010; or Hedin et al., 2014, 2016, etc.).*

    Yes, there is. We have included it as described above.

    You state in the abstract "Previous seismic investigations of the Seve Nappe Complex have shown indications for a strong but discontinuous reflectivity of this thrust zone, which is only poorly understood." Seeing this, as the reader I would expect a section / profile that shows that for the introduction.
    It's just nicer to know really where the borehole is located and the general stratification that has been worked out already (Lorenz et al., 2015a,b, 2019; Krauss et al., 2017; Wenning et al, 2017; etc.)

    Please, see comment above.

  - *Legend text, would be good to use emf-format; include reference to the map as a publication. The geological survey maps do in general have a publication reference.*

    We were not able to find any explicit map reference on the SGU webpage. However, the map is likely based on several mappings in the area over several years by different people (Lorenz, personal communication). With respect to Gee et al. (2010, Fig. 8) the map is most likely based on the geological map from Strömberg et al. (1994). We have added Strömberg et al. (1994) to the figure reference. Please, see also general comment to Figure 1, further above.

- ***Figure 2:***
  - *Please add referencing for the Downhole-logging data input.*

    Figure 2 is a generic explanation just to show the integration of the three methods (core, downhole logging and VSP) related to a specific physical parameter used in this study, namely the compressional wave velocity (Vp). We used velocity, because it was the common physical parameter for all three methods. This same method can be applied using other types of physical properties (e.g., density). So we prefer to not add additional references.

- *Could you indicate this in Figure 4, there would be enough space for the Core MSCL image, indicating the xyz structural axis to the foliation plane. Please see Figures 2 by Zappone et al. (2000).*

  We have indicated the core plug orientations and structural coordinates in Figure 2 as suggested. The figure capture text has been adjusted accordingly. Please also refer to comment on L104.

- ***Figure 4:***
  - *Please add reference for density log data source.*

    We have added the following reference:
    "Lorenz et al. (2015): COSC-1 operational report - Operational data sets GFZ Data Services."

- ***Figure 5:***
  - *Please add the reference that the method used is after Ji et al. (2007).*

    We have included the reference to Ji et al. (2007) and adjusted the labels inside the figure as described in the comment on L224.

    In addition, we have introduced a new figure (Figure 6) showing a data example used to derive the results as listed completely in Table 2.

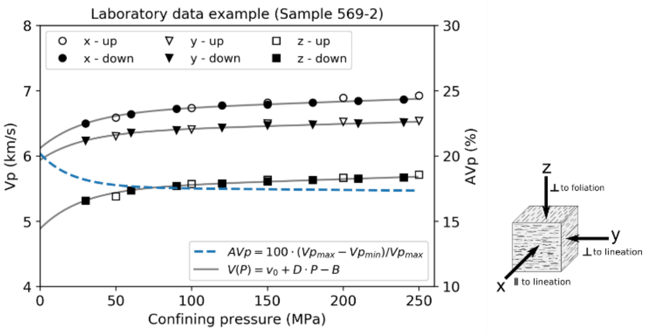

Figure 6: Data example showing confining pressure versus P-wave velocity (Vp) and anisotropy (AVp) for sample 569-2 (see Table 2). Open symbols refer to measurements during pressurization and filled symbols to measurements during depressurization. Different markers indicate the velocities measured on the respective x, y, and z core plugs along the corresponding structural axes (see also Fig. 5 and text for details).

- ***Figures 10 & 11:***
  - *Please increase text size in Figures 10 and 11 similar to Figure 12*

    We have increased the text size of Figure 12 (formerly Fig. 11).
    For Figure 11 (formerly Fig. 10), we prefer to keep the current text size to prevent overlapping labels. We will keep this in mind for the later publication process and will again check and optionally change it.

- ***Figure 12:***
  - *Please add the VpLP results to the plot.*

    We have added the mean VpAP as well as the VpLP results as small markers to the core and downhole log column, respectively, in Figure 13.

- *If it is not too much trouble, please add the legends on each figure, there is enough space.*

  We have added an additional legend to Figure 12.

  Elsewhere, we checked the legends that are included in the figure or, where more suitable, designated in the figure cation (e.g., Fig. 8, Fig. 9).

- ***Table 1:***
  - *Please add references to all downhole logging data that were not part of this study but used. This helps to keep this separate, what is new data and what is part of this study.*

    Yes, we have added the following two references to Table 1:
    "Lorenz et al. (2015): COSC-1 operational report - Operational data sets GFZ Data Services."
    "Krauß et al. (2015): Zero-Offset VSP in the COSC-1 borehole, Geophysical Research Abstracts."

<u>A few first questions that came to mind:</u>

- *How does the metamorphic facies Vp results compare to other similar projects (e.g. good comparison studies doi:10.1029/2006JB004867, 2007 or doi:10.1144/GSL.SP.1998.136.01.9, 1998)*

  We have added an additional paragraph to the discussion.

- *Uncertainty analysis is listed in references, but how was it implemented?*

  The uncertainty analysis was calculated based on a basic error propagation theory including the error of the sample specification for the velocity error. For the anisotropy uncertainty we propagated the model error of the regression coefficients to estimate the error. The uncertainty analysis was implemented using the python programming language, based on the fundamental equations described, e.g., by Taylor (1997). As being out of scope of this publication we kept the description of the error analysis to a sufficient limit in the submitted manuscript (see Methods). We prefer therefore to exclude too technical details (such as governing equations) that are, however, suitable for another more methodological publication.

- *As a connection to structural changes of the rock is mentioned as the primary reason for anisotropy, why not mark main structural intervals on Figure 10, if fractures have been analyzed?*

  We assess the structural interpretation in further below, at Figure 12. The main aim of figure 10 is to rather present results of the different log data yet without interpretation any lithological/structural differentiation.
  To understand who is driving the anisotropy, detailed analysis of the core samples has already been performed. XRD and microprobes analyses have been performed to understand if the mineralogical composition and structure can influence the anisotropy. This is the subject of the second paper. The manuscript will be submitted by the spring. The samples were also selected away from main fractures or veins that would have influenced the results of our analysis.

- *What is similar / different to the Chinese CCSD borehole experiment or the southern Iberian Peninsula? If dissimilar, are local settings governing the results? Just to mind the statement that this method would be a good tool for similar cases.*

  We have added a discussion about similar studies into the discussion.

Author response to reviewer 2

Referee: anonymous

Following the developments in resources exploration industry, scientific studies using core-log-seismic data integration were progressed gradually over three decades under the scientific drilling programs as standard use on almost every projects. However, quality of the data and integration process were limited on use of tools, operational difficulties, particularly in ocean drilling projects and for hard rocks. Hence, there are very few studies on hard rock data integration and this research is one of the few case using complete set of core, log and seismic data in high quality data as well as supported further experiment for integration.

We thank the reviewer for reviewing our manuscript submitted for publication in Solid Earth. The reviewer suggested a few minor modifications of the manuscript. According to the suggested amendments, we list the reviewer comments (RC2) and our proposed changes to the manuscript (AR) in the following:

L20:

RC2: Core-log-integration using synthetic seismograms requires wireline logging data and mafic lithologies.

AR: This is correct. This sentence is perhaps not clearly formulated. We removed it.

L167:

RC2: Rephrase to “[...] accuracy of the pulse arrival picks […]”

AR: Amended.

L208:

RC2: Remove “equals”

AR: Done.

L244:

RC2: Amend sentence to “[…] low values, agreeing well with the velocities measured on core […]”

AR: Amended.

L257:

RC2: Insert missing comma.

AR: Done.

L289:

RC2: Insert “with”

AR: Done.

L290:

RC2: Replace “the” with “these”

AR: Amended.

L328:

RC2: Rocks of the present study?

AR: Here, we are referring to the rocks found in the COSC-1 lithology. However, of course, this in particular is only true for the analyzed samples. We rephrased this for clarification: “This suggests a strong structural dependence of the seismic velocities for the rocks of the Seve Nappe drilled by the COSC-1 borehole.”

L335:

RC2: “Here”?

AR: We rephrased this line for clarification: “The presented anisotropy-depth profile […]”. We also added a reference to the referred figure.

L336:
RC2: Remove “Nevertheless”
AR: Amended sentence to: “Despite of large data gaps, […]”

L372:
RC2: Respell to “mantle-driven”
AR: Done.

L390:
RC2: Slightly low values or low values?
AR: Because of the insufficient closure microcracks we infer slightly lower velocities for the felsic gneisses than expected. We rephrased the sentence for clarification: “[…] result in lower values for […]”

L444:
RC2: “anisotrophies”
AR: We prefer to stay using always the singular and respelled it accordingly to “anisotropy” in the manuscript.

Correlation of core and downhole seismic velocities in high-pressure metamorphic rocks: A case study for the COSC-1 borehole, Sweden

Felix Kästner[1,2], Simona Pierdominici[1], Judith Elger[2], Alba Zappone[3], Jochem Kück[1], and Christian Berndt[2]

[1]Helmholtz Centre Potsdam, GFZ German Research Centre for Geosciences, 14473 Potsdam, Germany
[2]GEOMAR Helmholtz Centre for Ocean Research Kiel, 24148 Kiel, Germany
[3]ETH Zurich, Department of Earth Sciences, 8092 Zurich, Switzerland

Correspondence to: Felix Kästner (felix.kaestner@gfz-potsdam.de)

Abstract. Deeply rooted thrust zones are key features of tectonic processes and the evolution of mountain belts. Exhumed and deeply-eroded orogens like the Scandinavian Caledonides allow to study such systems from the surface. Previous seismic investigations of the Seve Nappe Complex have shown indications for a strong but discontinuous reflectivity of this thrust zone, which is only poorly understood. The correlation of seismic properties measured on borehole cores with surface seismic data can constrain the origin of this reflectivity. ~~In this study~~To this end, we compare seismic velocities measured on cores to in situ velocities measured in the borehole. For some intervals of the COSC-1 borehole, the ~~The~~ core and downhole velocities deviate by up to 2 km/s. ~~We suggest that~~These differences in the core and downhole velocities are most likely the result of microcracks mainly due to depressurization. However, the core and downhole velocities of the intervals with mafic rocks are generally in close agreement. S~~S~~eismic anisotropy measured on laboratory samples increases from about 5 to 26 % at depth, ~~indicating~~ correlating with a transition from gneissic to schistose foliation. Thus, ~~We suggest that differences in the core and downhole velocities are most likely the result of microcracks mainly due to depressurization. Thus, seismic velocity can help to identify mafic rocks on different scales whereas the velocity signature of other lithologies is obscured in core-derived velocities.~~ metamorphic foliation has a clear expression in seismic anisotropy. These results will aid in the evaluation of core-derived seismic properties of high-grade metamorphic rocks at the COSC-1 borehole and elsewhere. ~~In particular, they show that core log seismic integration via synthetic seismograms requires wireline logging data in any but mafic lithologies.~~

1 Introduction

Thrust zones in high-pressure metamorphic rocks are important features in mountain belts. In active fault zones they are often accompanied by devastating earthquakes like repeatedly occurring in the Himalayas (e.g., in 2015 [M=7.9] and 2008 [M=7.9]), which are a potential threat to the local population. Their investigation, therefore, is important to improve our understanding of the deeper orogenic processes and tectonic evolution.

However, such structures are seldom directly accessible and difficult to image. An exception are exhumed systems where most parts of the orogen were deeply eroded and exposed to upper crustal levels. The ~~Scandes~~ Caledonides ~~in~~ of western

Scandinavia, a remnant of the mid-Paleozoic Caledonian orogeny (e.g., Gee and Sturt, 1985), represent such a system ~~(e.g., Gee and Sturt, 1985)~~. Here, available geophysical investigations of an orogen root can be compared to geological and petrophysical observations from the surface (e.g., Ebbing et al., 2012). Reflection seismic data provide another possibility to investigate these thrust zones and revealed structures of a strong and highly diffuse reflectivity as, for example, observed at the highly metamorphic Seve Nappe Complex in the Jämtland region, in western Sweden (e.g., Hedin et al., 2012).

To better understand the origin of these reflections, one can compare them to the physical properties of the related rocks at depths to characterize the impact of structural and compositional variations on seismic properties. This involves comparison of seismic velocities from different measurements and scales with both lithological and structural characteristics of cored rocks.

In this study, we determine seismic properties on core scale (mm to cm) from the COSC-1 borehole in Jämtland, western Sweden (Fig. 1) and evaluate their potential to explain the in situ seismic properties (mm to km scale) by comparing core velocities with downhole logging data (cm to m scale) and core lithology. ~~Thereby~~Moreover, we focus on the effects of different ambient pressure conditions on the velocities, the potential impact of microcracks and fracturing as well as scale differences inherent in the individual data sets and measurement procedures (Fig. 2).

As core velocities measured under atmospheric pressure conditions can exhibit strong deviations from in situ conditions (Elbra et al., 2011), we integrate and compare the core and downhole seismic velocities with laboratory velocity and anisotropy results from 16 core samples measured under different confining pressure simulating in situ conditions. Ultimately, this results in better constrained seismic properties in the vicinity of the COSC-1 borehole, which is a prerequisite for a successful core-log-seismic data integration (Worthington, 1994).

The concept of integration and cross-calibration of data sets across different scales is well established in sedimentary basins of marine and lake environments (e.g., Bloomer and Mayer, 1997; Miller et al., 2013; Riedel et al., 2013; Thu et al., 2002), where it was successfully used to better characterize the subsurface seismic stratigraphy using both core and downhole logging data. But to date, there are only few studies that adapted this concept in hard-rock environments and similar metamorphic complexes. Some examples are the KTB borehole in Germany (Kern et al., 1991), the Kola superdeep borehole in Russia (Golovataya et al., 2006), the Chinese Continental Scientific Drilling borehole in China (Sun et al., 2012), or the Outokumpu deep drilling borehole in Finland (Kukkonen, 2011) ~~(e.g., Emmermann et al., 1990; Xu et al., 2009)~~.

The project COSC (Collisional Orogeny in the Scandinavian Caledonides) is a scientific drilling project co-funded by the International Continental Scientific Drilling Program (ICDP), the Swedish Research Council, and the Geological Survey of Sweden. It generally aims to study the mountain building processes of the Scandinavian Caledonides in western Sweden (Gee et al., 2010; Lorenz et al., 2015a). In 2014, the COSC-1 borehole was drilled in Åre-Jämtland (Fig. 1) to a total depth of 2495.8 m. It was fully cored below 103 m with almost 100 % core recovery. Drilling was accompanied by extensive field campaigns providing physical properties from downhole logs and ~~borehole and~~ seismic profiles (Hedin et al., 2014, 2016; Krauß et al., 2015; Lorenz et al., 2015a; Simon et al., 2015). Together with the excellent core recovery and data availability, the COSC-1 drilling project constitutes a perfect case study to apply core-log-seismic data integration in a metamorphic environment.

Commented [FK1]: Add reference to reflection profiles

Commented [FK2]: Add note on microcracks

Commented [FK3]: Move up to line line 35

Commented [FK4]: Add new paragraph

Commented [FK5]: COSC-1 drilling project

1.1 Geological Background

In the mid-Paleozoic, the Caledonian orogen formed during the continent-continent collision of Laurentia and Baltica (Gee et al., 2008). The Scandinavian Caledonides are composed of nappes that were thrusted over the Baltic platform margin accommodating several hundred kilometers of southeast-ward shortening. These thrust sheets are subdivided into the Lower, Middle, Upper, and Uppermost Allochthons, which rest on autochthonous crystalline basement (Fig 1; Gee et al., 2008; Roberts and Gee, 1985). The Lower Allochthon is mainly composed of sedimentary rocks of Upper Proterozoic to Silurian age derived from the outer Baltoscandian margin (Gee et al., 2010). The Middle Allochthon consists of several nappes with an increase in metamorphic grade, derived from the outer to outermost Baltoscandian margin including the continent-ocean transition zone (Gee et al., 2013). The uppermost part of the Middle Allochthon comprises the Seve Nappe Complex (SNC). The SNC is divided into a lower part of similar protolith to the underlying (greenschist facies) Särv Nappes but highly deformed in amphibolite and locally eclogite facies; a central part composed of granulite facies migmatites and paragneisses (e.g., Ladenberger et al., 2014), overlaid by an upper part of lower-metamorphosed sedimentary rocks (Gee et al., 2010). The Upper Allochthon is dominated by Early Paleozoic Iapetus-derived sedimentary rocks, ophiolites and volcanic arc complexes of greenschist facies. The Uppermost Allochthon is mostly composed of metasediments and carbonates from the Laurentian margin (Gee et al., 2008).~~While the Lower Allochthon is mainly composed of sedimentary rocks of Upper Proterozoic to Silurian age, the Middle Allochthon consists of rocks with an increase in metamorphic grade. The uppermost part of the Middle Allochthon comprises the Seve Nappe Complex (SNC). The SNC consists mainly of rocks of high metamorphic grade to amphibolite and locally eclogite facies (e.g., Ladenberger et al., 2014) derived from the sedimentary cover of the outer to outermost Baltoscandian platform margin including the continent-ocean transition zone (Gee et al., 2013). The Upper Allochthon consists of units of greenschist facies dominated by sedimentary rocks while the Uppermost Allochthon is mostly composed of metasediments and carbonates.~~

The dimension of the Caledonian mountain range and its formation mechanisms are similar to those of the more recently formed Himalayan orogen (Labrousse et al., 2010). Subsequent glaciation, tectonic uplift, and gravitational collapse left most parts of the mountain range deeply eroded exposing rock formations of middle to lower crust levels (Gee et al., 2008). Today's remnants, the Scandes, extend over a distance of about 300 km across the Scandinavian Peninsula, over a length of about 1700 km, from the Norwegian Skagerrak coast in the South up to the North Cape. An extensive review of the Caledonian Orogeny and related areas is provided by Corfu et al. (2014) and Gee and Sturt (1985).

Along the COSC-1 borehole, ~~B~~based on ~~first~~ the lithological descriptions of the cored rocks, four main sections were identified at depth (Lorenz et al., 2015a): (1) gneisses of varying compositions (mainly felsic, amphibolitic, calc-silicate), often garnet- and diopside-bearing, occur from top to about 1800 m; (2) an extensive (ductile shear) deformation zone prevails between 1800 and 2345 m; followed by (3) a 15 m-thick retrograde transition zone from amphibolite facies gneisses into lower-grade meta-sedimentary rocks; and (4) mylonitized quartzites and metasandstones of unclear tectonostratigraphic position that characterize the lowermost part to the bottom of the borehole at 2495 m.

Commented [FK6]: Refer to fig 1

Commented [FK7]: Revise tectonostratigraphy

The potential to investigate the deep structure of the orogenic root from the surface is directly addressed in the COSC ~~drilling~~ project. It generally focuses on the physical properties and inner structure of the emplaced nappe complex associated with high-grade metamorphic allochthonous rocks as well as the character and age of deformation of the underlying thrust sheets, the main Caledonian décollement, and the Precambrian basement (Gee et al., 2010; Lorenz et al., 2015a).

2 Data and Methods

For this study, we used compressional wave velocities from a multi-sensor core log (MSCL) and downhole ~~logging~~ data ~~from the COSC-1 borehole~~including a short-spacing sonic log (Lorenz et al., 2015b) and zero-offset vertical seismic profile (Krauß et al., 2015) from the COSC-1 borehole (see also Fig. 2). In addition, we measured selected core samples to provide seismic properties of characteristic lithological units. Based on these laboratory measurements, we calculated velocities at different environmental conditions (intrinsic, lithostatic pressure, and atmospheric pressure), which then served as a calibration tool for the core and downhole logging data. The individual data sets and experimental acquisition used for this study are described in the following subsections. Table 1 provides an overview of the individual measurements and related velocities, which nomenclature is used throughout this study.

2.1 Laboratory measurements

Laboratory analyses are routinely applied to study the elastic properties, fabric, and seismic anisotropy of crustal and mantle rocks (e.g., Barberini et al., 2007; Kern, 1982; Siegesmund et al., 1991; Zappone et al., 2000). We used seismic wave velocities measured on 16 core samples. These measurements were conducted at room temperature and varying confining pressure using the pulse-transmission method (Birch, 1960, 1961). In order to determine the seismic anisotropy, i.e., the directional dependence of seismic velocity, compressional (P) wave, the velocities were measured on three mutually perpendicular core plugs drilled out of each of the 16 core samples.

Six of these samples were measured by Wenning et al. (2016), chosen based on the most abundant lithologies derived from the lithological core description (Lorenz et al., 2015b). In order to extend and complement these measurements, we selected ten additional samples at depth intervals and lithologies that were not previously covered (see Table A1 for a detailed sample list). ~~We chose~~In general, the 16 samples ~~samples~~ cover a large depth range of the borehole including ~~from~~ potential zones of both higher and lower reflectivity as, for example, indicated by the zero-offset vertical seismic profile (Krauß et al., 2015).

The core samples were cut at lengths of about 15 to 20 cm from the COSC-1 drill cores. From each sample, we drilled three cylindrical core plugs of 3 to 5 cm length and 2.54 cm diameter (see also Fig. 2). The orientation of the plug axes *x*, *y*, and *z* agree with the major structural axes that are defined by the sample's foliation and lineation, and which we have determined by visual inspection. Following the common practice (Zappone et al., 2000), we designated *z* as the axis normal to the foliation plane. The foliation plane is spanned by the *x*- and *y*-axes, where *x* is oriented parallel and *y* perpendicular to the apparent lineation. The core plug ends were cut and ground to plane-parallel surfaces in order to provide a good coupling with the signal transducers. The plugs were oven-dried at 100 °C for at least 24 h in order to eliminate free water from the pore space.

The plug dimensions (length and diameter) and dry weight were determined using a micrometer caliper (+/- 0.01 mm) and precision balance (+/- 1e-3 g), respectively. We used the average diameter and length of four successive readings to reduce possible errors due to surface irregularities. The matrix density of each core plug was measured using a He-gas pycnometer (type: AccuPyc II 1340). This is based on a precise volume measurement using the gas displacement method (Lowell et al., 2004, p. 326).

The experimental procedure was similar to the one described in Wenning et al. (2016). For each core plug, ultra-sonic seismic velocities were acquired under different confining pressure using a hydrostatic pressure vessel and corresponding acquisition system (Fig. 3; Barblan, 1990). The setup consisted of two piezoelectric transducers (lead-zircon ceramics, 1 MHz resonance frequency), transmitter and receiver, which were placed on the core plug's cylinder faces. They were hold in place by a shrink tube jacketing plug and transducers. Additional metal wires, tightly wrapped around the shrink tube, sealed the core plug to prevent any oil leakage into it (Fig. 3). The prepared core plug was mounted inside the vessel where the oil pressure was applied and controlled using a pneumatic compressor. The pressure was first increased in 50 MPa steps, from 50 to 250 MPa, and then decreased in 30 MPa steps, between 240 and 30 MPa (±2 MPa). At each pressure step, a wave generator connected to one of the transducers produced an input square signal 0.2 microseconds wide, with an amplitude of 30 Volts, and a pulse rate of 0.5 kHz. Simultaneously, the wave generator sent a trigger signal with the same frequency to a PC-based wave analyzer. The analyzer used an impedance of 1 MΩ over a range of ±500 mV. The waveforms were recorded with a repetition rate of 80 ns and a sampling rate of 100 MHz. The electric noise was minimized by averaging the tracks.

The measurements were calibrated using steel cylinders of varying lengths to correct for the delay in the observed travel times (i.e., $t_{observed} = t_{rock} + t_{system}$), which was caused by the cables, transducers, and interfaces in the electronic system. The calibration was conducted at confining pressures of 50 and 100 MPa. The system travel time (t_{system}) was obtained by averaging the results from these two pressures.

We performed our measurements at room temperature (ca. 22 °C), which should be a good approximation of the in situ condition because of the very low geothermal gradient (ca. 20 °C/km) and low temperatures observed at about 2500 m, the bottom of the borehole (T_{log} < 60 °C; Lorenz et al., 2015b). Generally, seismic velocities decrease with temperature (e.g., Motra and Stutz, 2018; Schön, 1996). However, at very low temperatures (< 100 °C), like we observe in the COSC-1 borehole, this effect can be neglected (Kern, 1978). Moreover, the measured pressure to temperature increment (about 1.5 MPa/K) in the COSC-1 borehole is sufficiently high to prevent thermal microcracking (cf. Kern, 1990).

Commented [FK8]: Justify room temperatures
Add note on velocity-temperature behavior with references

In the subsequent data processing, we calculated velocities and anisotropy coefficients as a function of confining pressure for each core plug and sample, respectively. Because of a very good signal quality, it was not necessary to apply any additional filtering to the waveform data. First-arrival times were picked manually using a picking tool developed for this purpose (Grab et al., 2015). The seismic velocities were calculated using the plug length L, divided by the corrected travel time: $v = L / (t_{picked} - t_{system})$. Changes in the plug length due to compression can be neglected for these rock types (Zappone et al., 2000).

We calculated P-wave velocities at atmospheric and at lithostatic pressure to relate to the different conditions of the velocity measurements from downhole sonic, multi-sensor core logger (MSCL), and borehole seismic data. The lithostatic pressure was calculated from the core and downhole logging density and is shown together for the associated sample depths in Fig. 4. Since density was only logged down to about 1600 m, we used extrapolated densities down to 2500 m depth showing slightly higher pressures than those calculated from the core.

We used the relationship derived by Ji et al. (2007) to calculate P-wave velocity-pressure curves (Fig. 5) for each core plug of our 10 core samples ~~(Fig.)~~. This relationship consisted of a four-parameter exponential equation to relate the measured velocities to confining pressure by solving a least-squares curve-fitting problem (Fig. 5). The intrinsic velocity (Vp0), which corresponds to the undisturbed, crack-free rock matrix, was calculated from the intercept of the extrapolated linear part of the velocity-pressure relation. The velocities at room pressure (VpAP, p = 0.1 MPa) and lithostatic pressure (VpLP, p = Sv) were determined from the non-linear representation of the velocity-pressure relation (Fig. 5).

~~The six samples from~~ Wenning et al. (2016) ~~applied~~ used a slightly different relation for their six samples, ~~-~~proposed by Wepfer and Christensen (1991). For most applications aiming to determine the linear high-pressure part and intrinsic anisotropy both relations give consistent results. However, the inherent zero-boundary condition of Wepfer and Christensen's relation may lead to underestimated velocities in the extrapolated, non-linear low-pressure part, which is why we used the relationship by ~~(~~Ji et al.~~,~~ (2007) for our 10 samples, instead.

A full data example for one sample is shown in Fig. 6. It shows the measured P-wave velocities as a function of increasing and decreasing confining pressure for each of the three core plugs, and the velocity-pressure curves calculated from the downgoing pressure cycles.

The intrinsic seismic anisotropy (AVp) was determined from the Vp0 measured along the x, y and z directions (Fig. 6). In literature there are different representations of the velocity anisotropy (Birch, 1961; Crampin, 1989; Schön, 1996). These representations are generally based on a fractional difference of the maximum and minimum measured velocities but distinguish in the applied denominator. We used a definition after Crampin (1989), which is described by the degree of the fractional difference of the maximum and minimum velocity of the rock sample, i.e., $AVp = 100*(Vp_{max} - Vp_{min})/Vp_{max}$.

The main source of error in the determination of seismic velocity is the uncertainty in picking the first arrival times. We estimated a typical uncertainty in the picking of the P-wave first arrivals with an upper limit of $\delta t_{observed} \cong \pm 0.1$ µs. The seismic velocity uncertainty was estimated using the concept of error propagation (e.g., Taylor, 1997), providing an measured P-wave velocity uncertainty of $\delta Vp = \pm 0.11$ km/s on average. The uncertainty propagation in the extrapolated velocities at zero confining pressure ($\delta Vp0$) was based on the linear regression function that minimized the sum of the squared errors of the prediction. Subsequently, we used the error of the regression coefficients (i.e., slope and intercept) to derive the uncertainty for the anisotropy coefficient (AVp) using the same approach as for the measured velocities. The uncertainty of the P-wave anisotropy was below 1 % for all samples. Moreover, our error analysis has shown, that the bulk uncertainty of the measured seismic velocities is dominated by the pick ~~accuracy of the pulse arrivals~~accuracy of the pulse arrival picks, while errors in the plug length have only a minor impact.

Commented [FK9]: Clearify use of velocity-pressure relation

Commented [FK10]: Introduce data example with reference to (new) Fig. 6

Commented [FK11]: Clarify how these distinguish

2.2 Multi-sensor core log P-wave velocity

Seismic P-wave velocity was measured every 5 cm on the 2.5 km COSC-1 cores using an multi-sensor core logger (MSCL, type Geotek MSCL-S), which is based on automated full-waveform logging system (e.g., Breitzke and Spieß, 1993; Weber et al., 1997). The P-wave sensor setup comprised two signal transducers mounted on opposite sides, perpendicular to the core axis. The upper was a motor-driven piston transmitter, while the lower used a spring-loaded acoustic rolling contact (ARC), constantly pushed against the measured cores.

Commented [FK12]: Add references to general method

At each measuring position, a 230 kHz P-wave pulse was sent from the transmitter through the core and was recorded by the receiver. The recorded signal was pre-amplified, digitized, and sent to the acquisition software at a sampling frequency of 12.5 MHz. The first-arrival times were determined using a threshold method providing a user-defined threshold level and time delay. This system automatically determined the first excursion above the given threshold, after the delay. The total travel time (TOT) was then taken at the first zero-crossing. During the acquisition procedure, the voltage level (amplitude), threshold level, and time delay were adjusted ~~accordingly~~automatically, to ensure a good signal-to-noise ratio for the automatic picker.~~.~~ To provide a good coupling between the transducers and the core, the core surface was wetted before the measurement.

Furthermore, a calibration was carried out to determine the P-wave travel time offset (PTO), which accounts for the accumulated travel time delays through the transducer system (transducer faces, rubber plates, etc.). The actual travel time (TT) was derived by subtracting the PTO from total measured travel time, i.e., TT = TOT – PTO.

The calibration based on travel times measured on whole-round and half-split POM (*Polyoxymethylen*) cylinders of varying diameters (60 to 120 mm), which were plotted and extrapolated by a best linear fit. The P-wave velocities were calculated using the corrected travel time TT and the nominal core diameter (D = 61 and 47.6 mm), by Vp = D / (TOT – PTO) = D / TT. No additional temperature correction was applied because the room temperature inside the laboratory was kept constant at about 21 °C.

2.1 Downhole sonic logging

A downhole sonic measurement was carried out as part of a complete downhole logging campaign in 2014, about one month after the drilling of the COSC-1 borehole was completed. The original data set is published by Lorenz et al. (2015b, 2019) and comprises, amongst others, a density log and 3D core scan images. Downhole sonic velocities were continuously logged every 0.1 m by the Operational Support Group (OSG) of the ICDP using a standard full-waveform slimhole sonde (Antares, Germany). Transit times were calculated from first arrival times, which first were picked automatically and then refined manually. The seismic P-wave velocities were calculated using the sonde's receiver spacing (0.5 m) divided by the transit time.

Based on refracted waves propagating along the borehole wall, the sonic log represents a vertical average velocity of the near-well vicinity over the receiver spacing. The investigation depth and resolved rock volume generally depend on the formation velocities and frequencies, and can be estimated by three times the dominant wavelength (Serra, 1984). The frequency range of the recorded sonic traces lies in the order of a few kilohertz (Fig. 7). For the given sonde geometry and nominal transmitter frequency (20 kHz), the depth of investigation is about 0.75 to 1 m. Thus, downhole logging velocities provide a good approximation of the in situ seismic velocities, but can still be affected by micro-fracturing caused by drilling or steeply-dipping natural fractures.

2.2 Zero-offset vertical seismic profile

A zero-offset vertical seismic profile was acquired in the COSC-1 borehole, as part of a comprehensive post-drilling seismic survey to image the SNC and its underlying formations (Krauß, 2017; Krauß et al., 2015). In our study, we used the P-wave velocities that were calculated by the first-arrival times of the consecutive downhole receiver stations. The receiver spacing was 2 m and the first-arrival times were smoothed by a 15-point moving average (~~equals~~ 30 m interval) to account for small travel-time variations.

For a zero-offset (or rig-source) VSP, the direct P-wave ideally propagates downwards from the surface, parallel to the borehole. Thus, being relatively unaffected by the borehole itself, borehole-seismic velocities provide a good approximation of the vertical in situ seismic velocity of the borehole vicinity. The calculated, so called interval velocity represents the constant velocity of the seismic wave travelling through a rock layer with a given interval thickness, which is defined by the applied receiver spacing (2 m). Thus, the distance over which the velocity is averaged is four times larger than for the downhole sonic log (at 0.5 m receiver spacing).~~The distance over which the velocity was averaged was about 4 times larger than in the downhole sonic log.~~

Commented [FK13]: Rephrase for clarification

The signal frequencies ranged between 80 and 100 Hz (Fig. 7). The measurement scale was mainly dictated by the horizontal and vertical resolution. The former can be approximated by the first Fresnel zone of the dominant seismic wavelength. For the COSC-1 borehole range (0 to 2500 m), this yielded an average horizontal resolution of about 300 m (λ = 75 m, $v_{const.}$ = 6 km/s). In contrast, the vertical resolution was about 20 m, assuming one quarter of the dominant wavelength (~~best case~~Rayleigh resolution limit).

3 Results

3.1 Laboratory data

The laboratory intrinsic seismic velocities lie between 5.9 and 6.9 km/s showing generally little scattering (std = 0.3 km/s) throughout all samples (Table 2). The slowest velocities occur always along the z-axis, thus perpendicular to the foliation plane. Highest velocities occur in the foliation plane, i.e., along the x- and y-axes. The intrinsic seismic anisotropy exhibits a strong variation between 1 and 26 %, with an average error of 0.4 %. The average seismic anisotropy for all 16 samples is about 10 % (Table 2).

Velocities calculated at lithostatic pressure show values between 4.8 and 6.8 km/s (std = 0.5 km/s). Velocities calculated at atmospheric pressure are significantly lower, ranging from 1.5 to 5.7 km/s on average (std = 1.3 km/s). The measured sample densities vary between 2.7 and 3.1 g/cm³, with the highest densities observed for the amphibole-rich (mafic) samples (149-4, 193-2, 556-2, 631-1, and 661-3).

The mean intrinsic P-wave velocities (Vp0) were derived from the three axial (*x*, *y*, and *z*) core plug measurements (cf. Fig. 6). It~~the arithmetic mean of the three core plugs and~~ represents the most general case excluding any directional or structural effects and mainly account for the compositional effects (Fig. 8). Amphibole-rich (mafic) rock samples have velocities ranging between 6.5 and 6.9 km/s, whereas all other more felsic rock samples including the felsic gneisses, mica schists, and metasandstone, are characterized by a Vp0 between 6.0 and 6.4 km/s. The lowest Vp0 can be associated with the felsic gneiss samples, while the mica-rich schists show slightly higher Vp0. Moreover, both metasandstone (sample 664-2) and the carbonate-rich gneiss (sample 243-2) show very similar Vp0 as for the mica schists (e.g., samples 641-5, 651-5).

The seismic P-wave anisotropy (AVp) changes with increasing depth. This provides a simplified anisotropy-depth profile along the COSC-1 borehole (Fig. 9). The uppermost about 600 m show medium ~~anisotropies~~ anisotropy (<10 %) and low values (< 5 %) between 750 and 1500 m. Between 1600 and 1900 m, we observe the highest anisotropy effect with values up to 25 %, which decreases again, further below.

Comparing the different velocity distributions, the velocities at atmospheric pressure (VpAP) show very strong scattering and generally low values~~.~~, ~~These~~ agreeing well with the velocities measured on core under similar pressure conditions (Fig. 10). Velocities at lithostatic pressure (VpLP), in contrast, follow the in situ velocities measured downhole by the sonic ~~tool~~ and zero-offset VSP logs. On average, the intrinsic velocities (Vp0) are slightly higher than those calculated under lithostatic pressure.

3.1 Lab, core, and log data integration

Downhole sonic ~~log~~ and VSP logs show a good correlation, while VSP velocities have a lower resolution caused by the averaging. The raw core velocities show a strong scattering ~~with~~ and lower velocities on average (Fig. 10).

As we generally relate the core-derived data to measurements at surface conditions and the sonic and VSP logs to measurements under hydrostatic pressure in the borehole and the in situ rock (cf. Fig. 2), we expect the downhole measurements to show potentially higher velocities than those measured on core. Our data show that there ~~There~~ is neither a clear correlation between core and downhole velocities nor an observable static offset with depth (Fig. 11). There are places where the core-derived Vp increases while the downhole-measured Vp decreases, for example in the lowermost 200 m of the borehole. Moreover, we can observe core velocities that closely approach or even exceed the downhole velocities (430 to 780 m; 1700 to 2000 m), while at other depth intervals (620 m, 1640 m, and 1800 m)~~,~~ core and downhole Vp mismatch significantly. Between 160 and 180 m, we see a strong decrease in downhole P-wave velocities, which are likely related to a karstic unit previously recognized by a very high secondary porosity (Lorenz et al., 2015b). Here, the core and downhole velocities show a good agreement.

Commented [FK14]: Again point out which data refers to which condition

From about 430 to 780 m, we observe several peaks in the core velocities, which also correlate with peaks in the downhole velocity and density logs. Between 780 and 1900 m the core velocities gradually increase and they are accompanied by several smaller, less pronounced peaks, which often match with peaks in the downhole velocity and density logs (e.g., between 900 and 1000 m). From about 1900 m, down to about 2350 m, the core velocities tend to decrease, before they increase again abruptly and clearly approach the downhole velocities. Zones of clear opposite trends in the core velocities and downhole/VSP logs can be seen, for example, at 200 to 240 m, 600 to 625 m, 1200 to 1250 or, 1625 to 1650 m. These intervals encompass various core lithologies but most abundantly correlate with gneiss, calc-silicate rock, and amphibole gneiss.

In general, the superimposed mean sample velocities (intrinsic Vp0, atmospheric VpAP, and lithostatic VpLP) correlate well with the associated core (corresponds to VpAP) and downhole (corresponds to VpLP and Vp0) velocities. The sample densities match almost perfectly the core and downhole density measurements. While the mean intrinsic velocity Vp0~~ies~~ agree mostly with the downhole seismic velocities, they are slightly higher in some depth intervals (e.g., samples 193-2, 631-1), possibly due to anisotropy effects. The mean velocities calculated at lithostatic pressure (i.e., VpLP) are generally ~~follow~~ consistent with the downhole velocities ~~showing~~ and only show slightly lower values ~~in~~ for ~~the uppermost~~samples 106-1, 143-1, 243-2, and 361-2, which are located above about 1600 m ~~about 1600 m~~. Below about 1700 m, all samples ~~Below~~(except sample 631-1~~, they~~) ~~are~~ show very similar VpLP to the intrinsic velocities Vp0 (cf. Fig. 11, where markers are partly overlapped).

The velocities calculated at atmospheric pressure (i.e., VpAP) match the core velocities except for the samples 361-2, 556-2, 631-1, and 691-1. For samples 243-2 and 487-1 the mean velocities at atmospheric pressure are exceptionally low (1.7 and 1.5 km/s), thus, outside the displayed value range (see also Table 2).

At about 1750 and 1880 m, core and downhole velocities agree very well and the sample velocities (569-2 and 593-4) at atmospheric pressure are close to that at lithostatic pressure. Fracture mapping indicates a higher amount of low-angle fractures at these depths (Wenning et al., 2017). Moreover, these samples show the highest anisotropy values of all samples. We cannot observe any direct correlation of the foliation dips and the velocity data.

3.2 Comparison of velocity data at core scale

We conducted a detailed analysis of the measured seismic velocities at core scale (cm to mm), for six selected core sections (Fig. 12 a-f), which represent characteristic lithological units with respect to their seismic properties. We compared the measured core and downhole velocities with the laboratory results and correlated them with the unrolled 360° core scans (Lorenz et al., 2015b) of each selected core section. Missing core data are caused by samples taken previously to the core measurements.

Section 106-1 (Fig. 12 a) is a migmatite unit that is characterized by an alteration of darker restite bands and leucocratic melts (chemically very similar to felsic gneiss). Both core and downhole velocities are relatively stable showing an average difference of about 1.6 km/s. Sample velocities calculated at atmospheric conditions agree with the very low core Vp. The lithostatic velocity, however, is lower than those logged downhole, whereas the intrinsic velocities are higher. This indicates a strong effect of microcracks with poor orientation. The intrinsic seismic anisotropy is comparably low (< 5 %). Similar

Commented [FK15]: point out examples of depth intervals of opposite behavior:

Commented [FK16]: clarify the associated velocities by adding their corresponding abbreviations

Commented [FK17]: Add specific sample names as in the paragraph below results were obtained for ~~a~~the gneiss sample (e.g., sample 143-1; cf. Fig. 11~~, not shown~~), which have slightly higher core velocities (ca. 4.5 km/s) but similar downhole Vp (ca. 5.6 km/s).

Section 193-2 (Fig. 12 b) contains amphibolite where core and downhole velocities match well. We observe similar results for the metagabbro ~~sections~~ (~~e.g.,~~ sample 149-4, cf. Fig. 11~~, not shown~~), which are chemically almost equivalent. A fracture in the core section can be clearly identified by the core Vp. The velocit~~y~~ies at lithostatic pressure ~~-~~match~~es~~ almost perfectly with the downhole velocity, whereas~~. The very low~~ the velocities at atmospheric pressure ~~of the laboratory samples could be an artefact of an improper velocity-pressure relation for this sample~~are considerably lower than the associated core velocities. In comparison with the amphibolite sections, the metagabbro exhibits only slightly higher downhole velocities, which, however, still agree with velocities measured on core. In general, both units show very similar characteristics.

Section 361-2 (Fig. 12 c) is dominated by gneiss of felsic composition and shows similar characteristics as the uppermost gneiss sections (e.g., sample 143-1; cf. Fig. 11~~, not shown~~) and slightly higher velocities, which ~~could~~ possibly relates to an increase of mafic minerals such as amphibole. The core and downhole Vp differ strongly by up to 2 km/s.~~, while t~~The downhole velocities ~~are~~ lie around 6.2 km/s. A small amphibolite layer (<5 cm in thickness)~~,~~ can be well resolved by the core velocity. The core and downhole velocity of the surrounding gneiss unit ~~corresponds~~ agree well with the atmospheric velocity (VpAP) and the intrinsic velocity (Vp0), respectively.~~ It matches with the downhole measurements, which we interpret as an effect of closure of most microcracks at in situ lithostatic pressure.~~

Section 569-2 (Fig. 12 d) contains mostly mica schist. It exhibits the strongest anisotropy (15 to 20 %) of the cored rocks (see also Fig. 9). The core velocities (ca. 5 to 5.5 km/s) generally agree with the downhole velocities (ca. 5.5 km/s), being only slightly lower. The horizontal (*x*, *y*) plug velocities at atmospheric pressure ~~(see labels in figure)~~ are even higher than the downhole velocities and the ~~z component of the~~vertical (*z*) plug velocity at lithostatic pressure. However, the core velocities are still lower than the downhole velocities.

The amphibole-bearing gneisses of section 661-3 (Fig. 12 e) have relatively low core velocities of about 4.8 km/s. In contrast, the downhole velocities are very high (6.4 km/s), which agree well with the ~~z-component of the~~vertical (z) plug velocity at lithostatic pressure. The plug velocities at atmospheric pressure scatter strongly around the core velocities.~~ This suggests a strong effect of microcracks on the extracted core section.~~

The metasandstone section 664-2 (Fig. 12 f) is characterized by a very homogenous rock matrix and is predominately composed of quartz. The velocity anisotropy is very low (< 5 %). Both atmospheric and lithostatic velocity match well the corresponding core and downhole measurements. The present velocity differences are likely caused by microcracks, as indicated by the sample velocities. The core velocities for this section are almost constant (4.5 to 4.8 km/s), slightly higher than those measured in the uppermost felsic gneisses (see e.g., section 361-2 in Fig. 12 c).

4 Discussion

4.1 Laboratory seismic properties

Our laboratory investigations show that not only composition but also structural characteristics of the COSC-1 cores have a strong impact on seismic properties. Pechnig et al. (1997) showed that the physical properties of metamorphic rocks can be classified by both structure and composition. We have shown that samples from mafic rocks have average velocities higher than 6.5 km/s and densities above 2.9 g/cm³, whereas felsic gneisses and mica schists show lower P-wave velocities and densities of 2.7 to 2.8 g/cm³ (Table 2, Fig. 8). These results fit well with the characteristics observed on felsic and mafic rocks from the German Deep Drilling Program KTB (Bartetzko et al., 2005; Pechnig et al., 2005). We suggest that velocity contrasts mainly occur between the denser amphibole-rich units and the more felsic units including felsic gneisses, mica schists, and metasandstones.

Nevertheless, the mean intrinsic seismic velocity cannot clearly distinguish all investigated rock types probably because of very similar matrix velocities and rock compositions. Our results show that the P-wave seismic anisotropy provides additional information about the structural characteristics, which qualitatively correlates with the degree of foliation. We observed the highest ~~anisotropies~~ anisotropy (> 15 %) for the mica schists, which are characterized by a well-developed schistosity. In contrast, felsic gneisses and metasandstone samples showed a low ~~anisotropies~~ anisotropy of about 5 % or below. This suggests a strong structural dependence of the seismic velocities for the rocks of the Lower Seve Nappe drilled by the COSC-1 borehole.~~This suggests a strong structural dependence of the seismic velocities for the present rocks.~~

Assuming that the point measurements sufficiently represent the core, we distinguished four different zones based on the anisotropy depth profile (Fig. 9). They correspond to the following major lithological units~~Based on the anisotropy depth profile (Fig.), we can distinguish four different zones, which correspond to major lithological units~~: (1) medium-low AVp of alternating, very heterogeneous rock units (samples 106-1, ~~-~~143-1, 149-4, and 193-2;~~,~~ 400 to ~~-~~650 m), (2) very low AVp of felsic rocks with low schistosity (samples 243-2~~-to~~, 361-2, 487-1~~-487-1,~~; 790 to 1500 m), (3) high AVp of mica-rich rocks with well-developed schistosity (samples 5~~56~~69-2, ~~to 651-5~~593-4, 631-1, 641-5, 651-5 and 661-3~~,~~; 1690 to 2220 m), and (4) low AVp of granofelsic quartz-feldspar-rich rocks (sample 664-2, >2280 m). The lowermost depths were also not well constrained, being covered by only two samples, one metasandstone and one mica schist. According to the core description, however, most of the deepest (>2200 m) rock units are described as metasandstones with only a few layers of mica schist (Lorenz et al., 2015b). The presented anisotropy-depth profile (Fig. 9) is limited in resolution by the low number of samples. Despite of large data gaps, we are able to divide the borehole into structural units that are not detectable based on other seismic properties.

Rocks of the Seve Nappe Complex were subject to high- to ultrahigh pressure metamorphism (Arnbom, 1980; Klonowska et al., 2017; Majka et al., 2014), involving both structural and compositional changes of the protolith. Metamorphism may affect differently the seismic properties depending on the p-T history. Generally, we assume an increase in seismic velocity with increasing metamorphism due to compaction and formation of denser minerals. On the other hand, seismic anisotropy at

Commented [FK18]: State the samples precisely rock scale can either increase or decrease with increasing metamorphism due to crystallographic preferred orientation and dynamic recrystallization of constituent minerals under variable stress and temperature conditions (Bezacier et al., 2010; Falus et al., 2011; Keppler et al., 2017). We observed that for the upper 1.6 km of the COSC-1 borehole, the seismic anisotropy is lower for the high-grade gneisses and amphibolites while at greater depths (>1.6 km) high anisotropy is associated with lower-grade mica schists (Fig. 11, Fig. 12).

Laboratory studies (e.g., Babuska and Cara, 1991; Kern and Wenk, 1990; Shaocheng and Mainprice, 1988) have shown that seismic anisotropy can be affected by the degree of deformation, such as associated with high-strain rates and the mylonitization of rocks. Because of the associated lineation or stretching of minerals, this can favor an increase in the seismic anisotropy, as we observe, for example, for the amphibole-rich gneiss sample (sample 661-3, Fig. 9). However, from the core or log velocities alone, we are not able to find strong evidence for a shear zone interface or zones of mylonitic deformation. Better constraints of the effects of tectonic deformation at the sample scale require additional analysis of the microstructure and related anisotropy.

4.2 Seismic velocities under laboratory and in situ condition

We used sample velocities measured at increasing confining pressure using a hydrostatic pressure vessel (Fig. 3) to simulate velocities measured under atmospheric and downhole conditions. Based on velocity-pressure curves (Fig. 6), we calculated velocities that represent either intrinsic, core, or downhole logging conditions (Fig. 10).

For the uppermost samples, we observed higher intrinsic velocities than velocities calculated at their lithostatic pressure (Fig. 11). This is counter-intuitive because we would assume that the velocities calculated at lithostatic (i.e., in situ) pressure are higher or at least similar to those calculated at zero confining pressure. If this is not the case, the calculated lithostatic pressure is not high enough to exceed the non-linear (crack-related) part of the velocity-pressure relation. This implies that the in situ velocities for these rocks are stronger influenced by fractures or microcracks than the velocities of samples at greater depth in the borehole.

Both core velocity and core density, which we used to calculate the lithostatic pressure, were measured under dry-rock conditions. If compared with in situ measurements, the effect of (partial) saturation could explain why velocities are lower than under in situ conditions (e.g., Kingdon et al., 1998). However, Fountain (1976) showed that this effect should be negligible in crystalline rocks with low porosity such as those in this study. Very similar density values from the core and downhole measurements (Fig. 4) supports that water saturation does not have a big impact.

To simulate velocities under in situ pressure conditions, we calculated velocities at their lithostatic pressure (Fig. 4). This assumes that the principal stresses are equal in all directions and determined only by the overlying rock masses (e.g., Zang and Stephansson, 2010). But the in situ stress field can be more complicated due to tectonic processes such as ridge push, post-glacial relief, or ~~mantel~~mantle-driven stress. For the COSC-1 area, the in situ stress anisotropy is low (Wenning et al., 2017). Thus, we assume that lithostatic pressure is a good approximation for the in situ pressure conditions. This is further confirmed by the good correlation between the mean ~~velocities~~ velocities for 12 of the investigated 16 samples ~~calculated~~ at lithostatic pressure and the downhole logging velocities (cf. Fig. 10, Fig. 11~~)~~).

Low mean velocities at atmospheric pressure for some of the samples (Fig. 11: 361-2, 556-2, 631-1, and 691-1) could result from very low velocity in either one of the associated core plugs. This may result from insufficient data coverage of the low-pressure part of the velocity-pressure relation (cf. Fig. 5) causing wrong data extrapolation. Another source for such misfits is the different pressure relation used for the samples investigated by Wenning et al. (2016). This was based on the velocity pressure relationship proposed by Wepfer and Christensen (1991). This empirical relationship is adequate at higher pressures but not for zero confining pressure. Thus, velocities calculated at atmospheric pressure are generally too low.

We infer that the observed difference between intrinsic velocity and those calculated at lithostatic pressure is mainly caused by microcracks induced by anisotropic stress relaxation after coring downhole (e.g., Wolter and Berckhemer, 1989). Due to the insufficient closure of microcracks the onset of the linear part of the velocity-pressure curve is shifted to higher (p > 70 MPa) confining pressures whereas the calculated lithostatic pressure is located in the non-linear part. The fact that this effect mainly occurs in the uppermost, less schistose samples (e.g., 143-1, 361-2) suggests that these samples are more affected by microcracks and that in the schistose samples microcracks are more aligned and therefore can close faster under increasing pressure.

Our results suggest that the intrinsic seismic velocities are a good representation of the in situ seismic velocities as measured by downhole logging. Although the velocities calculated at lithostatic pressure generally agree with the downhole velocities, the insufficient closure of microcracks ~~leads to~~result in ~~slightly too~~ lower values for the felsic gneiss units.

4.3 Characteristics of core and downhole logging Vp measurements

Core and downhole velocity measurements using MSCL and sonic tools, respectively, are subject to different scales, sensor setup, and environmental conditions (Fig. 2). Other studies have shown that differences in seismic properties are generally due to depressurization and formation of microcracks after the core extraction (e.g., Wolter and Berckhemer, 1989; Zang et al., 1989). Especially in sedimentary rocks, the mechanical rebound of pore spaces due to decompression is a primary correction factor when comparing core to in situ data (Urmos et al., 1993). For crystalline, metamorphic rocks, the effect of volume expansion is relatively small. Microcracks can be either randomly distributed or show a preferred orientation relative to the rock microstructure or to the stress field around the borehole (Dresen and Guéguen, 2004; Nur and Simmons, 1969). Our simulation of velocities under crack-related and crack-free conditions (Fig. 5) indicate a strong influence of microcracks and a significant crack-induced anisotropy for certain rock samples (e.g., Fig. 12 a). This suggests that velocities measured on cores at atmospheric pressure are strongly affected by microcracking.

Fig. 11 illustrates the significant differences between the core and downhole seismic velocities at several depths. The discrepancy between the core and downhole logs can have different reasons. As discussed above, the decompression of the cores causes the formation of microcracks (asymmetric strain relaxation). With respect to the sample lithology (Table 2), we observe the strongest mismatch and lowest core velocities for the gneiss units. For the metasandstones, mica schists and mafic

Commented [FK19]: Point out the that X out of Y samples of VpLP show these results

Commented [FK20]: clarify

rocks the mismatch is comparably low and core velocities are increased. Especially, between about 450 and 800 m, core and downhole velocities matched very well, which coincides with mafic lithologies, i.e., metagabbros, amphibolites. These have higher densities, but they are probably also less affected by microcracks. We infer that microcracks impact more on the core velocities of the felsic gneisses than on other lithologies. Despite of the general mismatch in the core and downhole velocities, the core velocities resolve both large-scale and small-scale (less than about 5 cm) lithological changes that are related to mafic rocks (e.g., Fig. 12 c).

Other effects on the measured core velocities can be related to structural characteristics like the presence of dipping foliation, natural fractures, and grain boundary orientations. We show that MSCL measurements are sensitive to fractures in the rock resulting in too low velocities (see Fig. 12 b, d). Beside some naturally occurring fractures (see fracture column in Fig. 11; Wenning et al., 2017), most fractures are due to core handling and there are of course those that occur inevitably between each core section. In total, natural fractures and core section transition zones account for only about 10 % of the raw core data set suggesting that they are not the reason for the general mismatch. This is supported by the smoothed core velocities, where all such outliers were potentially removed (Fig. 11, smoothed core Vp profile).

The core data, unlike the downhole logging data, were acquired perpendicular to the core axis and, thus, parallel or sub-parallel to the metamorphic foliation (Fig. 2). In the presence of a well-developed foliation this would cause higher core velocities in horizontal direction, parallel to the foliation, as shown by our laboratory results where the fastest velocities always occur parallel to the foliation plane. However, at core scale and atmospheric pressure, this effect is less eminent and is only observed where a strong schistosity is present (Fig. 12 d).

The core and borehole velocity measurements were carried out using different frequencies ranging from a few 100 Hz for the VSP data to up to 1 MHz for the sample analyses (Fig. 7). In general, P-wave velocity and anisotropy dispersion may occur in porous and fractured rocks (Galvin and Gurevich, 2015; Thomsen, 1995). In absence of a fluid-saturated, equant porosity as in the case of mostly crystalline metamorphic rocks, P-wave dispersion can generally be neglected. Moreover, the different frequency scales are closely linked to the investigated rock volume, i.e., with increasing signal frequency the investigated rock volume generally decreases.

The seismic properties show considerable changes between each data set (Fig. 13). ~~Furthermore, there is no strong correlation between the lithological core description and the seismic velocities, which might be related to the very variable core lithology.~~Despite of no strong correlation between the core lithology and measured seismic velocities (cf. Fig. 11), we can observe ~~S~~some characteristic zones (Fig. 13) in the velocity profiles that can be linked to a general trend in the lithology, and which are consistent with the zones indicated by the anisotropy-depth profile as discussed earlier. Most eminent is the transition between the mafic, amphibole-rich rocks and the felsic gneisses at around 750 to 800 m. Overlying mafic units can be traced across all scales indicated by strong velocity contrasts and peaks between 400 and 800 m due to the layering of mafic and felsic rock units. In the MSCL data we can associate the low velocities with felsic gneisses, whereas the mica schists and metasandstones show slightly increased core velocities. While the differentiation of mica schists and gneisses, is very difficult due to the similar seismic velocities, high anisotropy values give indications for a unit dominated by mica schists, which also

Commented [FK21]: rephrase

Commented [FK22]: clarify and refer to zones determined by the anisotropy-depth profile, earlier in the discussion agrees with the lithological core description. This implies that the core-derived velocities cannot easily be used for core log seismic integration, both because they resolve the velocities at much greater resolution and because (in case of the MSCL data) they are too low due to decompression.

Core and log velocities suggest that velocity contrasts in the Lower Seve Nappe are mainly related to the mafic rock units, which are can be associated with boudinaged amphibolites (Hedin et al., 2016) or dolerite intrusions (Juhlin, 1990). We conclude that these mafic units predominately occur in the uppermost 800 m, in thick bands of 10 to 80 m, exhibiting intermediate intrinsic ~~anisotropies~~ anisotropy of up to 8 %. Potentially the core velocities can be used to derive a high-resolution reflectivity series with a high contrast level (dynamic range), which could help to better localize the origins of seismic reflections related to mafic units such as amphibolites and metagabbros.

Other studies in similar environments are for example by Ji et al. (2007), who focused on mafic/ultramafic rocks and orthogneisses from the CCSD project in the Dabie-Sulu ultrahigh pressure metamorphic terrane. They also showed a strong effect of microcracks caused by depressurization of the core material. Moreover, one can find a similar facies classification in terms of seismic velocities and anisotropy, where granitic gneisses exhibit lower Vp and AVp values than the ultramafic rocks. However, a direct comparison is only limited because they do not investigate lower grade metamorphic rocks such as mica schists. Another study on the Iberian Peninsula (Zappone et al., 2000), of two main metamorphic complexes (Nevado Filabride and Alpujharride), was an attempt to reconstruct a transect across a continental crust (from upper/middle to lower levels) using samples representative for lithologies of various composition and metamorphic facies from outcrops. The exposed crust in that region of Southern Spain, from Marbella to Ronda, shows a comparable large variability of rock types and an abundant component of high-temperature metamorphic rocks (up to migmatites). In contrast to the COSC-1 study, the Iberian study was conducted on outcrops, with rocks that went through an exhumation history up to exposition to atmospheric conditions (not the case in COSC-1). Moreover, most of the transect of the Alpujharride was representative of continental lower crust at the transition to the upper mantle, while in COSC-1 the rocks are of middle to crustal levels, i.e., only a few samples of the investigated units are compatible with the metamorphic conditions of the Seve Nappe. Thus, our results provide a valuable extension to the data base of rock properties from different metamorphic facies.

5 Conclusion

Integrating seismic properties from laboratory samples, core and downhole data helps to better define and distinguish seismic characteristics of the COSC-1 lithology. Our comparison of seismic velocity measurements across multiple scales, from laboratory to field, show that seismic P-wave velocities measured on cores can partly resolve in situ lithological variations. These are, however, not only influenced by compositional changes but also overprinted by metamorphic foliation and microstructures.

The investigated seismic properties allow to distinguish between at least three characteristic lithological units of the COSC-1 borehole: amphibolite/metagabbros, mica schists, and felsic gneisses. Although core velocities are affected by microcracks, they are able to resolve small scale features such as thin mafic layers (<5 cm) or sub-horizontal fractures. We were able to identify mafic units such as amphibolite by peaks in both core and downhole data, which can be used for lithological classification. Less prominent velocity contrasts but outstanding anisotropy values were observed for mica schists and metasandstones. Core and downhole velocity contrasts can be attributed to the transition from mafic to other lithologies, which dominates the uppermost borehole sections. Where core and downhole velocities show discrepancies this can be ascribed to microcracks induced by the coring process (strain relief of the core), and this occurs more frequently in the gneissic lithologies. The applied methods and presented results are a good tool for future case studies and extension to available data base.

6 Acknowledgement

Research funded by the Deutsche Forschungsgemeinschaft (DFG, German Research Foundation) – Project no. 339380967 (SPP-1006). The COSC-1 borehole was drilled with the Swedish national research infrastructure for scientific drilling, Riksriggen, and funded by the Swedish Scientific Drilling Program (SSDP) through the Swedish Research Council (VR-2013-94) and the International Continental Scientific Drilling Program (ICDP). We thank Bjarne Almqvist, Henning Lorenz, Iwona Klonowska, Jaroslaw Majka, Christopher Juhlin, and Ulrich Harms for constructive and fruitful discussions during manuscript preparation. We are grateful to Claudio Madonna and Quinn Wenning for providing their support and advice during the preparation and measurements of the samples at the Rock Deformation Laboratory of the ETH Zurich. We would like to thank Ulli Raschke for his assistance and efforts during core logging with the multi-sensor core logger at the BGR core repository in Berlin-Spandau, and Friederike Klos for providing logistical support for the sample material. Moreover, we thank Catalina Gebhardt for her advice on the processing of the MSCL data. We thank Anett Blischke and one anonymous reviewer for their valuable comments and suggestions, which have improved the manuscript considerably.

Commented [FK23]: add Riksriggen

7 References

Arnbom, J.-O.: Metamorphism of the Seve Nappes at Åreskutan, Swedish Caledonides, Geol. Föreningen i Stock. Förhandlingar, 102(4), 359–371, doi:10.1080/11035898009454493, 1980.

Babuska, V. and Cara, M.: Seismic anisotropy in the Earth, Kluwer Academic Publishers., 1991.

Barberini, V., Burlini, L. and Zappone, A.: Elastic properties, fabric and seismic anisotropy of amphibolites and their contribution to the lower crust reflectivity, Tectonophysics, 445(3–4), 227–244, doi:10.1016/J.TECTO.2007.08.017, 2007.

Barblan, F.: Paramètres physiques expérimentaux de roches de la croûte continentale intermédiaire à profonde, Université de Genève., 1990.

Bartetzko, A., Delius, H. and Pechnig, R.: Effect of compositional and structural variations on log responses of igneous and metamorphic rocks. I: mafic rocks, Geol. Soc. London, Spec. Publ., 240(1), 255–278, doi:10.1144/GSL.SP.2005.240.01.19, 2005.

Bezacier, L., Reynard, B., Bass, J. D., Wang, J. and Mainprice, D.: Elasticity of glaucophane, seismic velocities and anisotropy of the subducted oceanic crust, Tectonophysics, doi:10.1016/j.tecto.2010.09.011, 2010.

Birch, F.: The velocity of compressional waves in rocks to 10 kilobars: 1., J. Geophys. Res., 65(4), 1083–1102, doi:10.1029/JZ065i004p01083, 1960.

Birch, F.: The velocity of compressional waves in rocks to 10 kilobars: 2., J. Geophys. Res., 66(7), 2199–2224, doi:10.1029/JZ066i007p02199, 1961.

Bloomer, S. F. and Mayer, L. A.: Core-log-seismic integration as a framework for determining the basin-wide significance of regional reflectors in the eastern equatorial Pacific, Geophys. Res. Lett., 24(3), 321–324, doi:10.1029/96GL02076, 1997.

Breitzke, M. and Spieß, V.: An automated full waveform logging system for high-resolution P-wave profiles in marine sediments, Mar. Geophys. Res., 15(4), 297–321, doi:10.1007/BF01982387, 1993.

Corfu, F., Gasser, D. and Chew, D. M.: New perspectives on the Caledonides of Scandinavia and related areas: introduction, Geol. Soc. London, Spec. Publ., 390(1), 1–8, doi:10.1144/SP390.28, 2014.

Crampin, S.: Suggestions for a consistent terminology for seismic anisotropy, Geophys. Prospect., 37(7), 753–770, doi:10.1111/j.1365-2478.1989.tb02232.x, 1989.

Dresen, G. and Guéguen, Y.: Damage and Rock Physical Properties, in Mechanics of Fluid-Saturated Rocks, vol. 89, pp. 169–217, International Geophysics., 2004.

Ebbing, J., England, R. W., Korja, T., Lauritsen, T., Olesen, O., Stratford, W. and Weidle, C.: Structure of the Scandes lithosphere from surface to depth, Tectonophysics, 536–537, 1–24, doi:10.1016/J.TECTO.2012.02.016, 2012.

Elbra, T., Karlqvist, R., Lassila, I., Haeggström, E. and Pesonen, L. J.: Laboratory measurements of the seismic velocities and other petrophysical properties of the Outokumpu deep drill core samples, eastern Finland, Geophys. J. Int., 184(1), 405–415, doi:10.1111/j.1365-246X.2010.04845.x, 2011.

Falus, G., Tommasi, A. and Soustelle, V.: The effect of dynamic recrystallization on olivine crystal preferred orientations in mantle xenoliths deformed under varied stress conditions, J. Struct. Geol., 33(11), 1528–1540, doi:10.1016/J.JSG.2011.09.010, 2011.

Fountain, D. M.: The Ivrea—Verbano and Strona-Ceneri Zones, Northern Italy: A cross-section of the continental crust—New evidence from seismic velocities of rock samples, Tectonophysics, 33(1–2), 145–165, doi:10.1016/0040-1951(76)90054-8, 1976.

Galvin, R. J. and Gurevich, B.: Frequency-dependent anisotropy of porous rocks with aligned fractures, Geophys. Prospect., 63(1), 141–150, doi:10.1111/1365-2478.12177, 2015.

Gee, D., Fossen, H., Henriksen, N. and Higgins, A.: From the early Paleozoic platforms of Baltica and Laurentia to the Caledonide Orogen of Scandinavia and Greenland, Episodes, 31(1), 44–51, 2008.

Gee, D. G. and Sturt, B. A., Eds.: The Caledonide orogen: Scandinavia and related areas, Wiley., 1985.

Gee, D. G., Juhlin, C., Pascal, C. and Robinson, P.: Collisional Orogeny in the Scandinavian Caledonides (COSC), Gff, 132(1), 29–44, doi:10.1080/11035891003759188, 2010.

Gee, D. G., Janák, M., Majka, J., Robinson, P. and van Roermund, H.: Subduction along and within the baltoscandian margin during closing of the lapetus ocean and baltica-laurentia collision, Lithosphere, 5(2), 169–178, doi:10.1130/L220.1, 2013.

Golovataya, O. S., Gorbatsevich, F. F., Kern, H. and Popp, T.: Properties of some rocks from the section of the Kola ultradeep borehole as a function of the P-T parameters, Izv. Phys. Solid Earth, 42(11), 865–876, doi:10.1134/S1069351306110012, 2006.

Grab, M., Zürcher, B., Maurer, H. and Greenhalgh, S.: Seismic velocity structure of a fossilized Icelandic geothermal system: A combined laboratory and field study, Geothermics, 57, 84–94, doi:10.1016/J.GEOTHERMICS.2015.06.004, 2015.

Hedin, P., Juhlin, C. and Gee, D. G.: Seismic imaging of the Scandinavian Caledonides to define ICDP drilling sites, Tectonophysics, 554–557, 30–41, doi:10.1016/J.TECTO.2012.05.026, 2012.

Hedin, P., Malehmir, A., Gee, D. G., Juhlin, C. and Dyrelius, D.: 3D interpretation by integrating seismic and potential field data in the vicinity of the proposed COSC-1 drill site, central Swedish Caledonides, Geol. Soc. London, Spec. Publ., 390(1), 301–319, doi:10.1144/SP390.15, 2014.

Hedin, P., Almqvist, B., Berthet, T., Juhlin, C., Buske, S., Simon, H., Giese, R., Krauß, F., Rosberg, J. E. and Alm, P. G.: 3D reflection seismic imaging at the 2.5 km deep COSC-1 scientific borehole, central Scandinavian Caledonides, Tectonophysics, 689, 40–55, doi:10.1016/j.tecto.2015.12.013, 2016.

Ji, S., Wang, Q., Marcotte, D., Salisbury, M. H. and Xu, Z.: P wave velocities, anisotropy and hysteresis in ultrahigh-pressure metamorphic rocks as a function of confining pressure, J. Geophys. Res. Solid Earth, 112(9), B09204, doi:10.1029/2006JB004867, 2007.

Juhlin, C.: Interpretation of the reflections in the Siljan Ring area based on results from the Gravberg-1 borehole, Tectonophysics, 173(1–4), 345–360, doi:10.1016/0040-1951(90)90229-2, 1990.

Juhlin, C., Hedin, P., Gee, D. G., Lorenz, H., Kalscheuer, T. and Yan, P.: Seismic imaging in the eastern Scandinavian Caledonides: Siting the 2.5km deep COSC-2 borehole, central Sweden, Solid Earth, 7(3), 769–787, doi:10.5194/se-7-769-2016, 2016.

Keppler, R., Behrmann, J. H. and Stipp, M.: Textures of eclogites and blueschists from Syros island, Greece: Inferences for elastic anisotropy of subducted oceanic crust, J. Geophys. Res. Solid Earth, 122(7), 5306–5324, doi:10.1002/2017JB014181, 2017.

Kern, H.: The effect of high temperature and high confining pressure on compressional wave velocities in quartz-bearing and quartz-free igneous and metamorphic rocks, Tectonophysics, 44(1–4), 185–203, doi:10.1016/0040-1951(78)90070-7, 1978.

Kern, H.: Elastic-wave velocity in crustal and mantle rocks at high pressure and temperature: the role of the high-low quartz transition and of dehydration reactions, Phys. Earth Planet. Inter., 29(1), 12–23, doi:10.1016/0031-9201(82)90133-9, 1982.

Kern, H.: Laboratory seismic measurements: an aid in the interpretation of seismic field data, Terra Nov., 2(6), 617–628, doi:10.1111/j.1365-3121.1990.tb00127.x, 1990.

Kern, H. and Wenk, H. -R.: Fabric-related velocity anisotropy and shear wave splitting in rocks from the Santa Rosa Mylonite Zone, California, J. Geophys. Res. Solid Earth, 95(B7), 11213–11223, doi:10.1029/JB095IB07P11213, 1990.

Kern, H., Schmidt, R., Drilling, T. P.-S. and 1991, U.: The velocity and density structure of the 4000 m crustal segment at the KTB drilling site and their relationship to lithological and microstructural, Sci. Drill., 2, 130–145, 1991.

Kingdon, A., Rogers, S. F., Evans, C. J. and Brereton, N. R.: The comparison of core and geophysical log measurements obtained in the Nirex investigation of the Sellafield region, Geol. Soc. London, Spec. Publ., 136(1), 97–113, doi:10.1144/GSL.SP.1998.136.01.9, 1998.

Klonowska, I., Janák, M., Majka, J., Petrík, I., Froitzheim, N., Gee, D. G. and Sasinková, V.: Microdiamond on Åreskutan confirms regional UHP metamorphism in the Seve Nappe Complex of the Scandinavian Caledonides, J. Metamorph. Geol., 35(5), 541–564, doi:10.1111/jmg.12244, 2017.

Krauß, F.: Combination of Borehole Seismic and Downhole Logging to Investigate the Vicinity of the COSC-1 Borehole in Western Scandinavia, TU Bergakademie Freiberg., 2017.

Krauß, F., Simon, H., Giese, R., Buske, S., Hedin, P. and Juhlin, C.: Zero-Offset VSP in the COSC-1 borehole, Geophys. Res. Abstr., 17(EGU2015-3255), 2015.

Kukkonen, I. T., Ed.: Outkumpu Deep Drilling Project 2003-2011., 2011.

Labrousse, L., Hetényi, G., Raimbourg, H., Jolivet, L. and Andersen, T. B.: Initiation of crustal-scale thrusts triggered by metamorphic reactions at depth: Insights from a comparison between the Himalayas and Scandinavian Caledonides, Tectonics, 29(5), n/a-n/a, doi:10.1029/2009TC002602, 2010.

Ladenberger, A., Be’eri-Shlevin, Y., Claesson, S., Gee, D. G., Majka, J. and Romanova, I. V.: Tectonometamorphic evolution of the Åreskutan Nappe – Caledonian history revealed by SIMS U–Pb zircon geochronology, Geol. Soc. London, Spec. Publ., 390(1), 337–368, doi:10.1144/SP390.10, 2014.

Lorenz, H., Rosberg, J.-E., Juhlin, C., Bjelm, L., Almqvist, B. S. G., Berthet, T., Conze, R., Gee, D. G., Klonowska, I., Pascal, C., Pedersen, K., Roberts, N. M. W. and Tsang, C.-F.: COSC-1 – drilling of a subduction-related allochthon in the Palaeozoic Caledonide orogen of Scandinavia, Sci. Drill., 19, 1–11, doi:10.5194/sd-19-1-2015, 2015a.

Lorenz, H., Rosberg, J.-E., Juhlin, C., Bjelm, L., Almqvist, B., Berthet, T., Conze, R., Gee, D. G., Klonowska, I., Pascal, C., Pedersen, K., Roberts, N. and Tsang, C.: COSC-1 operational report - Operational data sets., 2015b.

Lorenz, H., Rosberg, J.-E., Juhlin, C., Bjelm, L., Almqvist, B., Berthet, T., Conze, R., Gee, D. G., Klonowska, I., Pascal, C., Pedersen, K., Roberts, N. and Tsang, C.: COSC-1 operational report - Operational data sets (V. 1.2), GFZ Data Serv., doi:10.5880/ICDP.5054.002, 2019.

Lowell, S., Shields, J. E., Thomas, M. A. and Thommes, M.: Characterization of Porous Solids and Powders: Surface Area, Pore Size and Density, 1st ed., Springer Netherlands, Dordrecht., 2004.

Majka, J., Rosén, Å., Janák, M., Froitzheim, N., Klonowska, I., Manecki, M., Sasinková, V. and Yoshida, K.: Microdiamond discovered in the Seve Nappe (Scandinavian Caledonides) and its exhumation by the “vacuum-cleaner” mechanism, Geology, 42(12), 1107–1110, doi:10.1130/G36108.1, 2014.

Miller, K., Browning, J. V., Mountain, G. S., Bassetti, M. A., Monteverde, D., Katz, M. E., Inwood, J., Lofi, J. and Proust, J.-N.: Sequence boundaries are impedance contrasts: Core-seismic-log integration of Oligocene–Miocene sequences, New Jersey shallow shelf, Geosphere, 9(5), 1257, doi:10.1130/GES00858.1, 2013.

Motra, H. B. and Stutz, H. H.: Geomechanical Rock Properties Using Pressure and Temperature Dependence of Elastic P- and S-Wave Velocities, Geotech. Geol. Eng., 36(6), 3751–3766, doi:10.1007/s10706-018-0569-9, 2018.

Nur, A. and Simmons, G.: Stress-induced velocity anisotropy in rock: An experimental study, J. Geophys. Res., 74(27), 6667–6674, doi:10.1029/JB074i027p06667, 1969.

Pechnig, R., Haverkamp, S., Wohlenberg, J., Zimmermann, G. and Burkhardt, H.: Integrated log interpretation in the German Continental Deep Drilling Program: Lithology, porosity, and fracture zones, J. Geophys. Res. Solid Earth, 102(B8), 18363–18390, doi:10.1029/96JB03802, 1997.

Pechnig, R., Delius, H. and Bartetzko, A.: Effect of compositional variations on log responses of igneous and metamorphic rocks. II: Acid and intermediate rocks, Geol. Soc. Spec. Publ., 240, 279–300, doi:10.1144/GSL.SP.2005.240.01.20, 2005.

Riedel, M., Bahk, J. J., Kim, H. S., Yoo, D. G., Kim, W. S. and Ryu, B. J.: Seismic facies analyses as aid in regional gas hydrate assessments. Part-I: Classification analyses, Mar. Pet. Geol., 47, 248–268, doi:10.1016/j.marpetgeo.2013.04.011, 2013.

Roberts, D. and Gee, D. G.: An introduction to the structure of the Scandinavian Caledonides, in The Caledonide Orogen: Scandinavia and Related Areas, edited by D. G. Gee and B. A. Sturt, pp. 55–68., 1985.

Schön, J.: Physical properties of rocks : fundamentals and principles of petrophysics, Pergamon., 1996.

Serra, O.: Fundamentals of Well-Log Interpretation 1. The Acquisition of Logging Data, Elsevier., 1984.

Shaocheng, J. and Mainprice, D.: Natural deformation fabrics of plagioclase: implications for slip systems and seismic anisotropy, Tectonophysics, doi:10.1016/0040-1951(88)90153-9, 1988.

Siegesmund, S., Kern, H. and Vollbrecht, A.: The effect of oriented microcracks on seismic velocities in an ultramylonite, Tectonophysics, 186(3–4), 241–251, doi:10.1016/0040-1951(91)90361-U, 1991.

Simon, H., Krauß, F., Hedin, P., Buske, S., Giese, R. and Juhlin, C.: A combined surface and borehole seismic survey at the COSC-1 borehole, Geophys. Res. Abstr., 17, EGU-4554, 2015.

Strömberg, A., Karis, L., Zachrisson, E., Sjöstrand, T. and Skogland, R.: Bedrock Geological Map of Jämtland County (Caledonides), scale 1:200 000, Sveriges Geol. Undersökning, Ca 53, 1994.

Sun, S., Ji, S., Wang, Q., Xu, Z., Salisbury, M. and Long, C.: Seismic velocities and anisotropy of core samples from the Chinese Continental Scientific Drilling borehole in the Sulu UHP terrane, eastern China, J. Geophys. Res. Solid Earth, 117(B1), n/a-n/a, doi:10.1029/2011JB008672, 2012.

Taylor, J.: An introduction to error analysis : the study of uncertainties in physical measurements, University Science Books., 1997.

Thomsen, L.: Elastic anisotropy due to aligned cracks in porous rock, Geophys. Prospect., 43(6), 805–829, doi:10.1111/j.1365-2478.1995.tb00282.x, 1995.

Thu, M. K., Tamaki, K., Kuramoto, S.-I., Tada, R. and Saito, S.: High-resolution seismic stratigraphy of the Yamato Basin, Japan Sea and its geological application, Isl. Arc, 11(1), 61–78, doi:10.1046/j.1440-1738.2002.00352.x, 2002.

Urmos, J., Wilkens, R. H., Bassinot, F., Lyle, M., Marsters, J. C., Mayer, L. A. and Mosher, D. C.: Laboratory and Well-Log Velocity and Density Measurements from the Ontong Java Plateau: New In-Situ Corrections to Laboratory Data for Pelagic Carbonates, in Proceedings of the Ocean Drilling Program, 130 Scientific Results, vol. 130, pp. 607–622, Ocean Drilling Program., 1993.

Weber, M. E., Niessen, F., Kuhn, G. and Wiedicke, M.: Calibration and application of marine sedimentary physical properties using a multi-sensor core logger, Mar. Geol., 136(3–4), 151–172, doi:10.1016/S0025-3227(96)00071-0, 1997.

Wenning, Q. C., Almqvist, B., Hedin, P. and Zappone, A.: Seismic anisotropy in mid to lower orogenic crust: Insights from laboratory measurements of Vp and Vs in drill core from central Scandinavian Caledonides, Tectonophysics, 692(A), 14–28, doi:10.1016/j.tecto.2016.07.002, 2016.

Wenning, Q. C., Berthet, T., Ask, M., Zappone, A., Rosberg, J.-E. and Almqvist, B. S. G.: Image log analysis of in situ stress orientation, breakout growth, and natural geologic structures to 2.5 km depth in central Scandinavian Caledonides: Results from the COSC-1 borehole, J. Geophys. Res. Solid Earth, 122(5), 3999–4019, doi:10.1002/2016JB013776, 2017.

Wepfer, W. W. and Christensen, N. I.: A seismic velocity-confining pressure relation, with applications, Int. J. Rock Mech. Min. Sci. Geomech. Abstr., 28(5), 451–456, doi:10.1016/0148-9062(91)90083-X, 1991.

Wolter, K. E. and Berckhemer, H.: Time dependent strain recovery of cores from the KTB - Deep drill hole, Rock Mech. Rock Eng., 22(4), 273–287, doi:10.1007/BF01262283, 1989.

Worthington, P. F.: Effective integration of core and log data, Mar. Pet. Geol., 11(4), 457–466, doi:10.1016/0264-8172(94)90079-5, 1994.

Zang, A. and Stephansson, O.: Stress Field of the Earth’s Crust, Springer Netherlands., 2010.

Zang, A., Wolter, K. and Berckhemer, H.: Strain recovery, microcracks and elastic anisotropy of drill cores from KTB deep well, Sci. Drill., 1(3), 115–126, 1989.

Zappone, A., Fernàndez, M., García-Dueñas, V. and Burlini, L.: Laboratory measurements of seismic P-wave velocities on rocks from the Betic chain (southern Iberian Peninsula), Tectonophysics, 317(3–4), 259–272, doi:10.1016/S0040-1951(99)00319-4, 2000.

8 Data availability

All core and downhole logging data are available through the ICDP data repository (cosc.icdp-online.org) and are referenced in the text with the respective data publication. The newly acquired data will be curated by the ICDP data repository (http://doi.org/10.5880/ICDP.5054.002).

9 Sample availability

Each of the 16 core samples has an IGSN (see Table A1). The samples are stored at the individual institutes and can be requested from the authors.

10 Author contribution

FK and SP carried out the core measurements. FK and AZ conducted the laboratory measurements and analysis. FK prepared the manuscript with contributions from all co-authors. SP and CB are responsible for conceptualization and funding acquisition. All authors worked on the manuscript.

11 Competing interests

The authors declare that they have no conflict of interest.

12 Figures

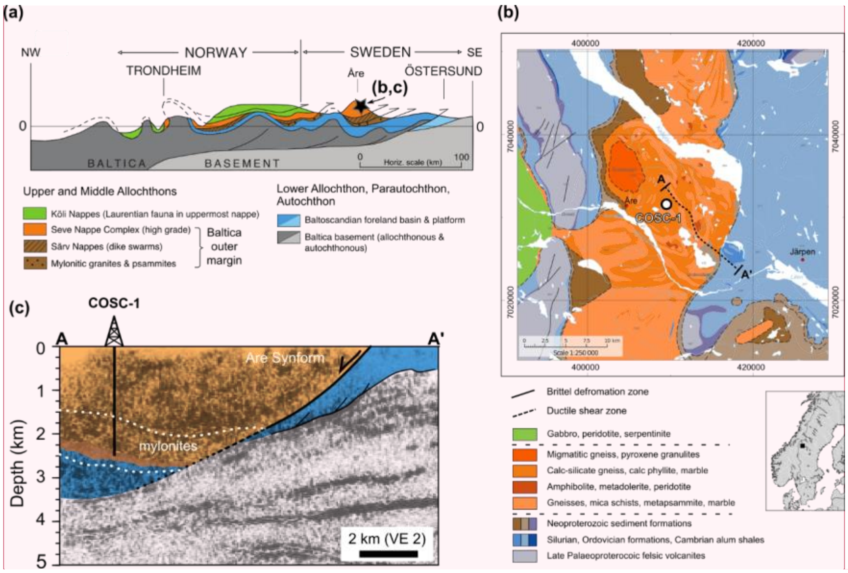

~~Figure~~Fig. 1~~1~~. Overview of the regional setting and study area. (a) Tectonostratigraphic division of the central Scandinavian Caledonides (Gee et al., 2010; Lorenz et al., 2015a); (b) Bedrock map with location of the COSC-1 borehole (colors modified; SGU Map Service; ~~(~~Strömberg et al., 1994~~)~~); (c) Seismic cross-section indicated in (b) showing a part of the COSC seismic profile (Hedin et al., 2012) with the COSC-1 borehole penetrating the highly reflective Lower Seve Nappe (adapted from Juhlin et al., 2016)~~Geological map of the Åre-Järpen area in western Scandinavia (see inset) showing the COSC-1 borehole location (circle marker). Bedrock map from Geological Survey of Sweden (SGU)~~.

Commented [FK24]: Add revised figure with geological background and cross-section

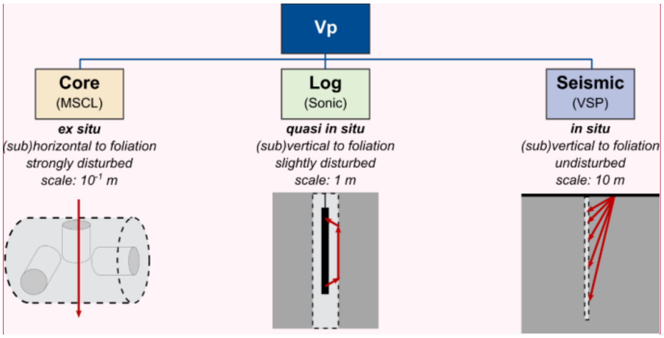

Commented [FK25]: Indicate core plugs

~~Figure~~Fig. 2~~2~~. Schematic depicting the different environmental and measurement conditions of the core, log, and borehole seismic (VSP) P-wave velocity (Vp) measurement. Arrows indicate the direction of seismic wave propagation.

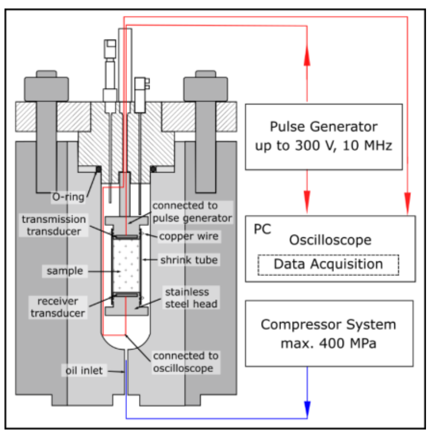

~~Figure~~Fig. 3~~3~~. Schematic of the experimental setup used to determine the P-wave velocities under confining pressure. This setup comprises a pressure vessel with a sample chamber, pulse generator, compressor control, and PC-based acquisition unit. Placed inside the oil-filled pressure chamber there is the sample assembly (Barblan, 1990).

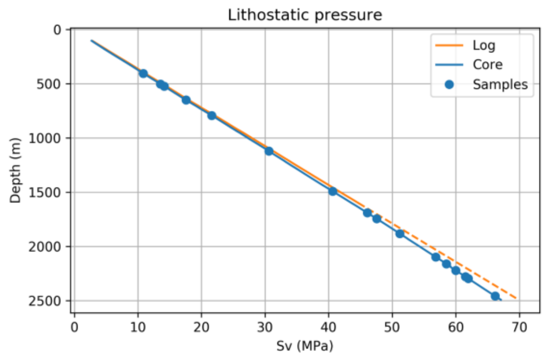

~~Figure~~Fig. ~~4~~4. Lithostatic pressure curve of the COSC-1 borehole derived from core and downhole density measurements (Lorenz et al., 2015b). The values for the 16 core samples are marked accordingly. The dashed line was linearly extrapolated since downhole density was only logged down to about 1.6 km.

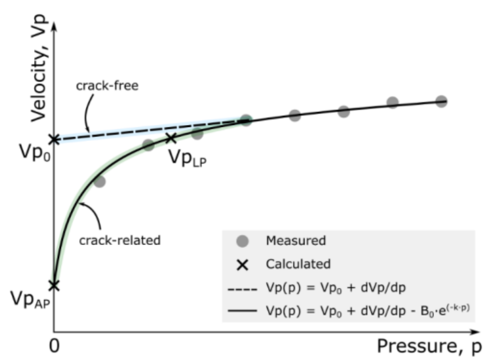

~~Figure~~Fig. 5. Schematic ~~V~~velocity-pressure relation depicting the measured and calculated seismic P-wave velocity Vp as a function of confining pressure p. Based on the best curve fit for the linear (dashed line) and non-linear part (solid line), velocities can be calculated under different environmental conditions: Vp_0 – intrinsic velocity, Vp_{AP} – atmospheric pressure, Vp_{LP} – lithostatic pressure (adapted from Ji et al., 2007).

Commented [FK26]: Add reference

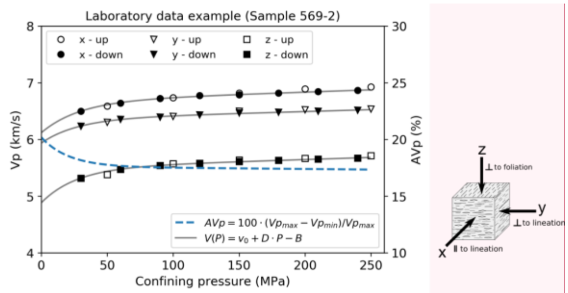

~~Figure~~Fig. 6. Data example showing confining pressure versus P-wave velocity (Vp) and anisotropy (AVp) for sample 569-2 (see Table 2). Open symbols refer to measurements during pressurization and filled symbols to measurements during depressurization. Different markers indicate the velocities measured on the respective x, y, and z core plugs along the corresponding structural axes (see also Fig. 5 and text for details).

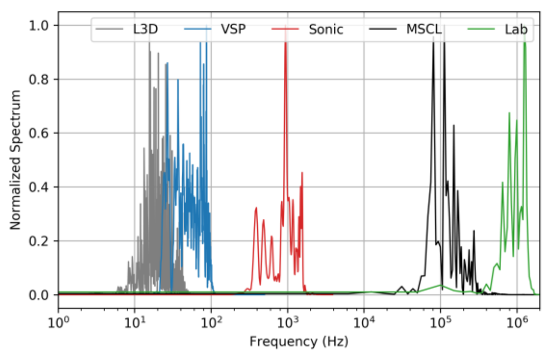

~~Figure~~Fig. 7~~6~~. Comparison of frequency spectra of seismic measurements across multiple scales from limited 3D surface seismic (L3D), borehole seismic (VSP), downhole log (sonic), core measurement (MSCL), and laboratory samples (Lab). The downhole-related spectra are calculated from a single seismic trace and sonic waveform extracted from approximately the same downhole depth of about 500 m.

Commented [FK27]: Insert data example showing measured data and structural reference frame

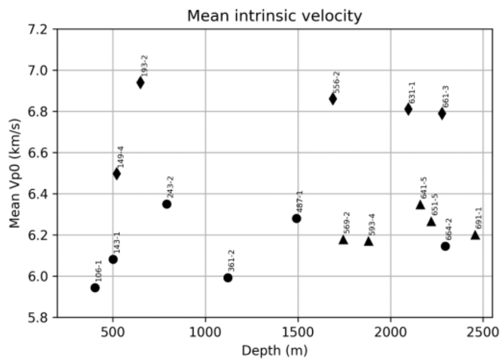

~~Figure~~Fig. 8~~7~~. Mean intrinsic velocity measured on 16 core samples from the COSC-1 borehole plotted at the respective sample depth. Markers correspond to simplified lithological classes such as mafic amphibole-rich units (♦), felsic gneisses/metasandstones (●), and mica schist (▲). Note that the highest values occur for the mafic lithologies.

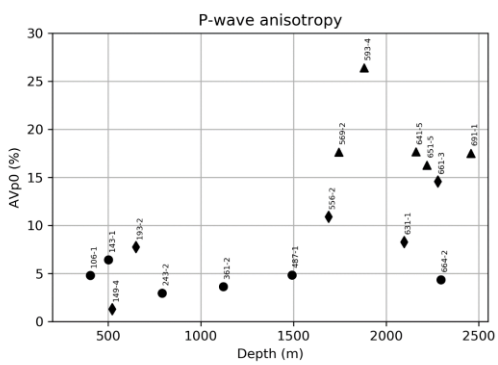

~~Figure~~Fig. 9~~8~~. Seismic anisotropy measured on 16 rock samples from the COSC-1 borehole plotted at the respective sample depth. Markers correspond to simplified lithological classes such as mafic amphibole-rich units (♦), felsic gneisses/metasandstones (●), and mica schist (▲).

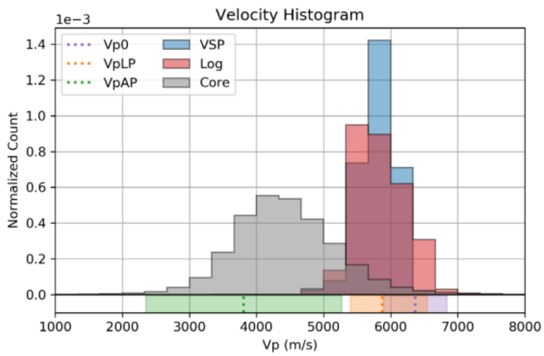

775

~~Figure~~Fig. 109. Distribution of P-wave velocities derived from laboratory samples (Vp0, VpLP, VpAp), core measurements (Core), downhole logging (Log), and borehole seismic (VSP). The sample velocities are displayed below the histograms indicating the mean and standard deviation of the 16 laboratory core samples.

Commented [FK28]: consider to change y-axis

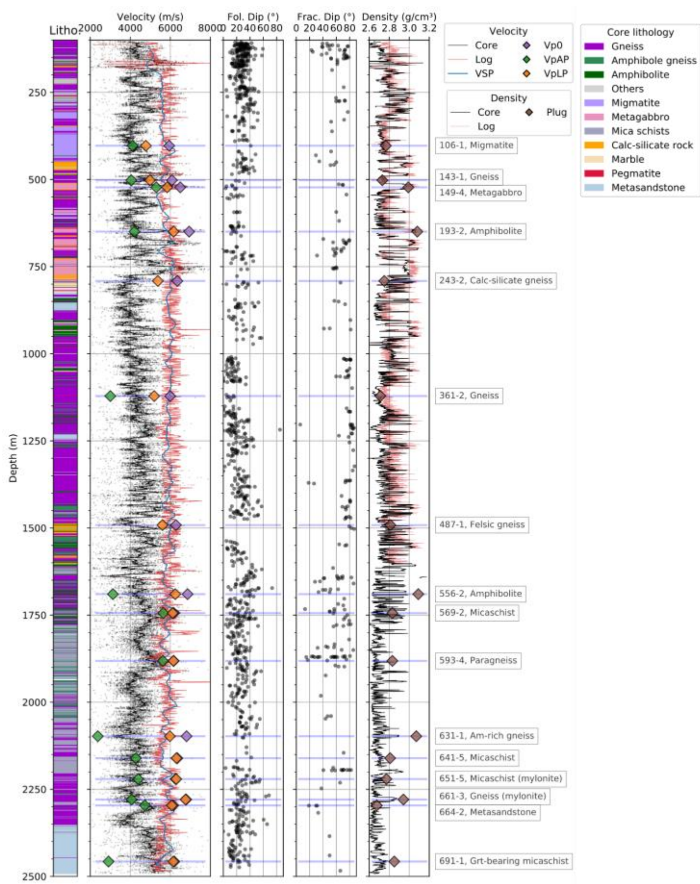

~~Figure~~Fig. 11~~10~~. Core-log data integration of the seismic properties alongside with the fracture and foliation dips (Wenning et al., 2017) in the COSC-1 borehole. The sample velocity and density data are superimposed on the respective log panels. The lithology is based on the COSC-1 lithological description of the core (modified after Lorenz et al., 2015b). VSP velocities are based on the zero-offset vertical seismic profiling data (Krauß et al., 2015).

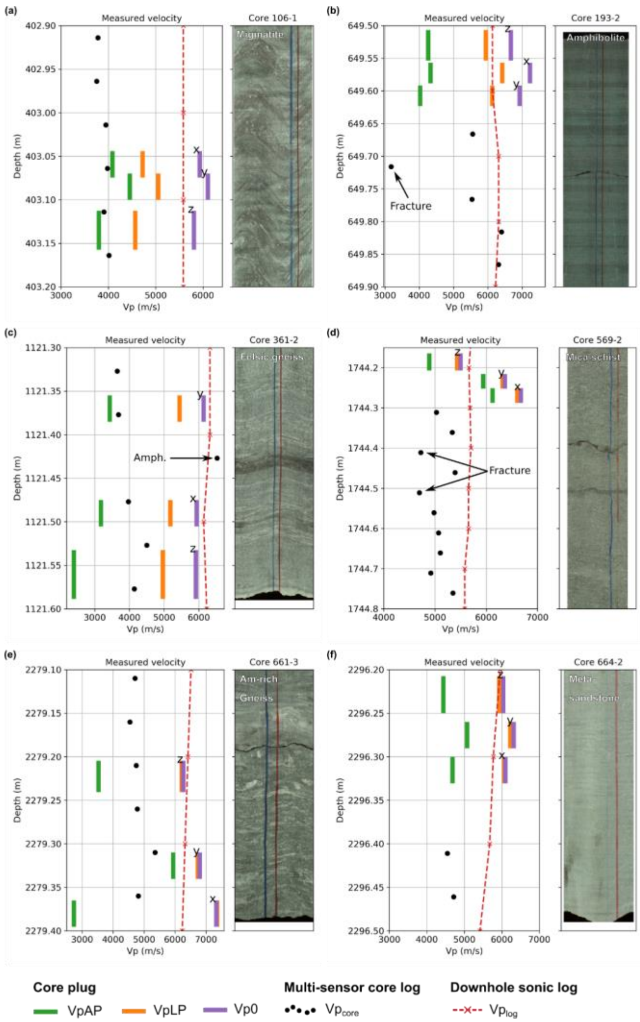

~~Figure~~Fig. 12~~11~~. Comparison of P-wave velocities across different scales. A-F) Laboratory sample, core measurements and downhole sonic velocities are shown next to the unrolled, true-color core scans. The colored bars represent the location of the three plug locations ~~(for colors refer to previous figures)~~; black dots: core velocity from MSCL, red dashed line: downhole sonic velocity. The blue and red lines on the core images are common practice to indicate the top and bottom of the core.

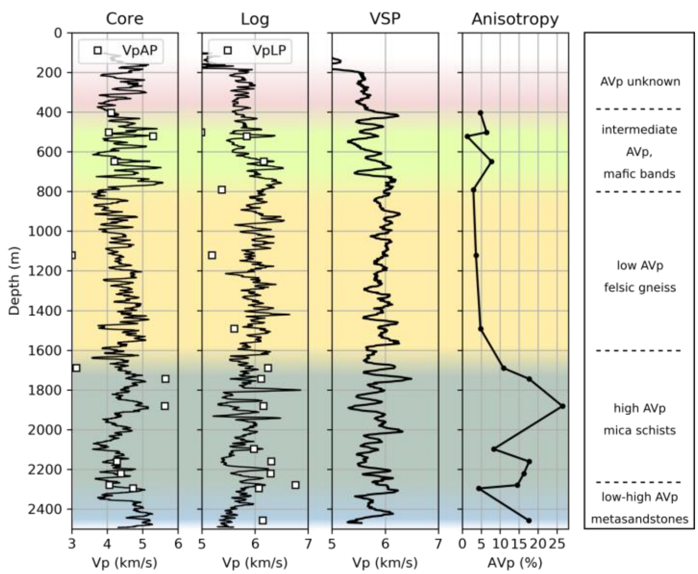

~~Figure~~Fig. 13~~12~~. Up-scaled core, log, and borehole seismic (VSP) velocities together with the laboratory-derived anisotropy-depth profile. Core and downhole logging velocities are smoothed over a 10 m average and superimposed by the mean sample velocities (markers) calculated at atmospheric (VpAP) and lithostatic (VpLP) pressure. The anisotropy profile is linearly interpolated (see also Fig. 9~~Fig. 7~~). The colored sections highlight characteristic velocity zones based on the resultant data sets shown here.

13 Tables

Table 1. Overview of velocity nomenclature used in this study. The laboratory measurements were carried out on three mutually perpendicular core plugs. See text for details.

Commented [FK29]: add data references

Velocity	Type of measurement	Direction of measurement	Description
Vp0	Lab	triaxial	Intrinsic P-wave velocity based on laboratory measurements on core plugs
VpAP	Lab	triaxial	P-wave velocity calculated at atmospheric pressure (p = 0.1 MPa) based on laboratory measurements on core plugs
VpLP	Lab	triaxial	P-wave velocity calculated at lithostatic pressure (p = Sv(z)) based on laboratory measurements on core plugs
Vpcore	MSCL	perpendicular to core axis	P-wave velocity continuously measured on whole cores using a multi-sensor core logger
Vplog	Downhole sonic	parallel to borehole axis	P-wave velocity continuously logged downhole using a short-spacing sonic sonde (Lorenz et al., 2015b)
VpVSP	Borehole seismic	parallel to borehole axis	P-wave velocities measured downhole using a zero-offset vertical seismic profile (Krauß et al., 2015)

Table 2. Laboratory data of 16 rock samples from the COSC-1 borehole. Sv - Lithostatic pressure derived from core density.

Sample	Core Lithology	Depth (m)	Density (g/cm³)	Sv (MPa)	Intrinsic velocity Vp0 (km/s)				Intrinsic anisotropy (%)		Extrinsic velocity VpAP (km/s)				Lithostatic velocity VpLP (km/s)			
					x	y	z	Mean	AVp~~0~~	Error	x	y	z	Mean	x	y	z	Mean
106-1	Migmatite	403.09	2.76	10.83	5.93	6.10	5.81	5.94	4.79	0.35	4.08	4.45	3.80	4.11	4.72	5.05	4.56	4.78
143-1	Gneiss	502.10	2.73	13.56	6.09	6.28	5.87	6.08	6.44	0.62	3.91	4.51	3.73	4.05	4.94	5.28	4.73	4.98
149-4	Metagabbro	522.41	2.99	14.13	6.53	6.52	6.44	6.50	1.29	0.67	6.38	5.83	3.68	5.30	6.44	6.06	5.02	5.84
193-2*	Amphibolite	649.59	3.08	17.58	7.23	6.93	6.67	6.94	7.75	*NA*	4.33	4.03	4.27	4.21	6.42	6.13	5.95	6.17
243-2*	Calc-silicate gneiss	791.22	2.75	21.59	6.44	6.37	6.25	6.35	2.95	NA	1.50	2.40	1.04	1.65	5.40	5.55	5.18	5.38
361-2	Gneiss	1121.48	2.71	30.61	5.93	6.13	5.91	5.99	3.63	0.92	3.18	3.43	2.40	3.00	5.18	5.44	4.96	5.19
487-1*	Felsic gneiss	1491.72	2.81	40.63	6.42	6.31	6.11	6.28	4.83	*NA*	1.66	1.40	1.40	1.49	5.75	5.65	5.42	5.61
556-2*	Amphibolite	1689.94	3.09	46.08	7.25	6.88	6.46	6.86	10.90	*NA*	4.73	2.65	2.02	3.13	6.81	6.36	5.57	6.25
569-2	Mica schist	1744.27	2.83	47.55	6.67	6.36	5.50	6.18	17.63	0.18	6.12	5.94	4.89	5.65	6.60	6.32	5.43	6.12
593-4	Paragneiss	1881.51	2.83	51.18	6.90	6.52	5.08	6.17	26.41	0.17	6.50	6.08	4.29	5.63	6.89	6.47	5.10	6.16
631-1*	Am-rich gneiss	2097.65	3.07	56.87	7.12	6.78	6.53	6.81	8.29	*NA*	3.22	2.13	1.78	2.38	6.27	6.04	5.62	5.98
641-5	Mica schist	2160.64	2.81	58.53	6.92	6.41	5.70	6.35	17.65	0.56	4.37	4.93	3.53	4.28	6.98	6.36	5.57	6.31
651-5	Mica schist (mylonite)	2220.52	2.77	59.97	6.74	6.41	5.64	6.27	16.27	0.27	5.58	5.08	2.51	4.39	6.76	6.46	5.66	6.30
661-3	Am-rich gneiss (mylonite)	2279.31	2.94	61.53	7.32	6.79	6.26	6.79	14.56	0.34	2.74	5.94	3.53	4.07	7.35	6.73	6.21	6.76
664-2	Metasandstone	2296.29	2.68	61.97	6.09	6.31	6.04	6.15	4.36	0.13	4.68	5.07	4.44	4.73	6.06	6.22	5.93	6.07
691-1*	Grt-bearing mica schist	2457.26	2.85	66.17	6.42	6.68	5.51	6.20	17.51	*NA*	2.45	3.69	2.59	2.91	6.41	6.54	5.49	6.15

*) Samples measured by Wenning et al. (2016), AVp data recalculated~~.~~

14 Appendices

Table A1. List of investigated core samples, their exact core position, and associated International Geo Sampling Number (IGSN). The section tops refer to the meter-corrected depth from the operation data sets (Lorenz et al., 2019). FK – samples newly measured for this study; QW – samples originally measured by Wenning et al. (2016).

Core	Section	Box	Slot	Section Top (m)	Sample Top (cm)	Sample Bottom (cm)	Examiner	IGSN
106	1	102	1	402.80	20	40	FK	BGRB5054RXG9401
143	1	135	1	501.76	20	40	FK	BGRB5054RXI9401
149	4	141	4	522.22	9	29	FK	ICDP5054EXK6601
193	2	184	2	649.51	0	15	QW	ICDP5054EXL6601
243	2	233	2	790.49	65	80	QW	ICDP5054EXN6601
361	2	343	3	1120.76	55	82.6	FK	BGRB5054RXP9401
487	1	467	1	1490.97	62	87	QW	ICDP5054EXS6601
556	2	528	3	1689.84	0	20	QW	ICDP5054EXU6601
569	2	542	3	1743.89	27	42	FK	ICDP5054EXV6601
593	4	575	4	1880.83	60	75	FK	ICDP5054EX47601
631	1	627	5	2096.96	60	78	QW	ICDP5054EXY6601
641	5	642	4	2160.49	0	20	FK	BGRB5054RXY9401
651	5	656	1	2220.29	10	30	FK	BGRB5054RX0A401
661	3	669	4	2278.43	77	95.8	FK	BGRB5054RX1A401
664	2	673	4	2295.51	70	85	FK	ICDP5054EX6A601
691	1	711	2	2456.64	54	69	QW	ICDP5054EX27601